Physics of Fluids ARTICLE scitation.org/journal/phf

Turbulence and scale relativity

Cite as: Phys. Fluids 31, 105109 (2019); doi: 10.1063/1.5108631
Submitted: 13 May 2019 • Accepted: 16 September 2019 •
Published Online: 22 October 2019 • Publisher error corrected: 20 November 2019

View Online Export Citation CrossMark

Laurent Nottale[a)] and Thierry Lehner[a)]

AFFILIATIONS

LUTH, Observatoire de Paris-Meudon, F-92195 Meudon Cedex, France

[a)]laurent.nottale@obspm.fr and thierry.lehner@obspm.fr

ABSTRACT

We develop a new formalism for the study of turbulence using the scale relativity framework (applied in v-space, following de Montera's proposal). We first review some of the various ingredients which are at the heart of the scale relativity approach (scale dependence and fractality, chaotic paths, irreversibility) and recall that they indeed characterize fully developed turbulent flows. Then, we show that, in this framework, the time derivative of the Navier-Stokes equation can be transformed into a macroscopic Schrödinger-like equation. The local velocity Probability Distribution Function (PDF), $P_v(v)$, is given by the squared modulus of a solution of this equation. This implies the presence of null minima $P_v(v_i) \approx 0$ in this PDF. We also predict a new acceleration component, $A_q(v) = \pm\mathcal{D}_v\, \partial_v \ln P_v$, which is divergent in these minima. Then, we check these theoretical predictions by data analysis of available turbulence experiments: (1) Empty zones are in effect detected in observed Lagrangian velocity PDFs. (2) A direct proof of the existence of the new acceleration component is obtained by identifying it in the data of a laboratory turbulence experiment. (3) It precisely accounts for the intermittent bursts of the acceleration observed in experiments, separated by calm zones which correspond to $A_q \approx 0$ and are shown to remain perfectly Gaussian. (4) Moreover, the shape of the acceleration PDF can be analytically predicted from A_q, and this theoretical PDF precisely fits the experimental data, including the large tails. (5) Finally, numerical simulations of this new process allow us to recover the observed autocorrelation functions of acceleration magnitude and the exponents of structure functions.

I. INTRODUCTION

Turbulence is a complex dynamical phenomenon which involves the coupling of many scales together. Its understanding is "one of the greatest challenges of modern physics."[1,2] Turbulent fluids can be seen as spatiotemporal chaotic systems involving a lot of coupled degrees of freedom. This has prevented their description in terms of the theory of low dimensionality chaotic dynamical systems. Moreover, they are out of equilibrium systems. This is manifested through the existence of a cascade of energy flux[3] connecting the various scales. This cascade is conveyed through a multiscale organization of eddies through their fragmentation (direct cascade) or fusion (inverse cascade).

Although the underlying (Navier-Stokes) equations are deterministic, turbulent flows are so complex phenomena that most of their components are usually considered to being fully random and thus described by stochastic tools. However, one of the main goals of the present paper amounts to show that some components of the Lagrangian acceleration are partly deterministic and behave as pseudorandom variables.

The physical consequences of the cascade were first explored by Kolmogorov (K41).[4] He found that there is an "inertial" range of scales in which the eddies are too large for viscosity to be important and too small to retain any effect of large-scale inhomogeneities. The Navier-Stokes equations are invariant to scaling transformations in this inertial domain (see, e.g., Ref. 1), which ranges from the dissipative small scale (η, τ_η) to the integral large scale (L, T_L) of energy input. In that range, fundamental scaling relations have been found by Kolmogorov for velocity increments, $\delta v \sim \delta x^{1/3}$ (Eulerian) and $\delta v \sim \delta t^{1/2}$ (Lagrangian)[5] under the hypothesis of an invariant energy transfer ε between eddies of different scales. We shall see that this universal Lagrangian K41 scaling also plays a leading role in the present work, interpreted as fractality (of fractal dimension 2) in velocity space.[6]

One of the main unsolved properties of fully developed turbulence is intermittency. It manifests itself as an alternance of calm periods and bursts of intense activity for accelerations or velocity increments. One of its signatures is the existence of very large tails of the acceleration probability distribution (PDF), which have been experimentally measured up to more than 50 standard deviations.[7]

Another signature is the differences experimentally observed for exponents of structure functions with the K41 expectation. Several stochastic models have been designed to account for this intermittency, beginning with Kolmogorov (K62),[8] in particular, multifractal random walks.[1,9–14] These models are based on some experimentally observed specific features (such as correlation functions) but are not dynamical solutions of the Navier-Stokes equations. The problem of intermittency remains a subject of ongoing active research.[15–17] In the present paper, we suggest an alternative solution to the intermittency problem, involving the effective dynamics and thus accounting for its various characteristics.

The theory of scale relativity,[18–20] on its side, has been constructed for describing explicitly scale dependent (in particular fractal[21]) physical phenomena. For this purpose, it introduces scales in an explicit way, both in variables and equations. In its framework, one looks for the form taken by the equation of dynamics in a fractal and nondifferentiable geometry. One finds that it can be integrated under the form of a Schrödinger-type equation.

Various ingredients of standard quantum mechanics were recovered and demonstrated from this approach:[18,22,19] in particular, the wave function is just a manifestation of the velocity field of the fluid of geodesics in a fractal space, and the Schrödinger equation is an integral of the equation of geodesics, re-expressed in terms of this wave function.

It appeared that the theory could also be applied, as an approximation, to chaotic macroscopic systems.[18,23,19] Indeed, a Schrödinger-type equation can be obtained from the equations of dynamics under just three conditions:[18,19] (i) infinite number of potential paths, (ii) fractality of each path (with fractal dimension 2), and (iii) local irreversibility under reflection of the time increment ($\delta t \leftrightarrow -\delta t$).

This led us to suggest that a fractal medium could simulate, at some level, a fractal space, and that particles moving in such a medium could therefore acquire macroscopic quantum-type properties; hence, we wrote as early as 1993 (Ref. 18, Chap. 7) “such a (fractal) medium should show very unusual properties, e.g., a quasiquantum coherent behavior at macroscopic scales.”

Actually, the theory of scale relativity, when it is applied at the fundamental level (i.e., as an attempt of theoretical foundation of standard quantum mechanics) introduces a fractal space (more generally space-time) as a generalization of the curved space-time of general relativity. In this case, “fractal space” denotes a purely geometrical entity, defined at the inter-relational level (as described, e.g., by a metric relation), but without any specific substance. The main idea here is that if a (now material) medium owns the same kind of fractal and nondifferentiable properties, it would play for the objects moving into it the role played by a fractal space on the objects it contains.

The open question since that time was therefore to find such a medium in natural systems or to build it in a laboratory experiment. However, such systems are expected to be fractal only on a limited range of scales. Two additional constraints should be added to the three above conditions for manifesting such a macroscopic Schrödinger regime: (iv) a large enough range of fractal scales (Ref. 19, Chap. 10) and (v) Newtonian dynamics. Indeed, in the application of the theory to quantum mechanics, we considered that space-time was fractal and nondifferentiable below the de Broglie scale, without any lower limit, and the dynamics is naturally Newtonian. However, when it is applied to a fractal medium instead of a fractal space, a lower scale is expected for its fractality, and the diffusive aspects of the medium may involve a Langevin-type dynamics instead of a Newtonian one. This reduces the number of systems where such a new physics could be implemented.

One of the natural realms to search for such properties at the observational level was therefore astrophysics, which provides one with both fractal systems on large ranges of scales and Newtonian/Einsteinian dynamics, since their formation and evolution are dominated by gravitation. Then, a large body of indirect proofs of a macroscopic Schrödinger regime has been revealed for many astrophysical systems on many scales, from planetary systems to extragalactic scales (Ref. 18, Chap. 7.2)[24,23,25] and (Ref. 19, Chap. 13). Other suggestions of possible implementations of such a new physics have been made in biophysics[26–28] but also in solid state physics where it could be involved in the unusual properties of high temperature superconductors.[29,30]

However, a direct proof from a laboratory experiment was still lacking. It has been suggested by Montera[6] that such a proof could be found in a fully developed turbulent fluid, but in velocity-space instead of position-space. Indeed, the above five conditions are fulfilled for such a fluid, but condition (ii) applies for velocity increments instead of space increments, under the Kolmogorov (K41) inertial scaling relation $\delta v^2 \sim \delta t$ which corresponds to fractal dimension 2 in v-space. Moreover, it is known that this relation holds between the integral scale T_L at large scales and the dissipative Kolmogorov scale τ_η at small scales and that their ratio (i.e., the range of fractal scales) is given by $T_L/\tau_\eta \approx R_\lambda/2C_0$ in terms of the reduced Reynolds number $R_\lambda = \sqrt{15 R_e}$. Here, C_0 is the Kolmogorov constant in the Lagrangian velocity autocorrelation function, and $D_2(\tau) = C_0 \varepsilon \tau$, where ε is the rate of energy dissipation, leading to the K41 relation $C_0 \varepsilon = 2\sigma_v^2/T_L$. With $C_0 \approx 4$,[31] one obtains a scale ratio of 100 for $R_\lambda = 800$, while the turbulence is considered to be fully developed beyond $R_\lambda \approx 500$.[32] Finally, being described by the Navier-Stokes equations, the dynamics is essentially Newtonian, at least in the inertial range, although it becomes dominated by the diffusion term $\nu \Delta v$ at small dissipative scales, at which the scaling behavior ceases.

Another strong argument for the application of the scale relativity approach to a fully turbulent fluid is that it is directly adapted to the Lagrangian description of such a fluid (and therefore to a comparison with Lagrangian experiments). Indeed, one obtains the Schrödinger-type description[22] by identifying the wave function with a manifestation of the velocity field of fractal geodesics.[18]

Numerical simulations of fractal geodesics[33] (Ref. 19, Chap. 10) have been performed in the context of standard quantum mechanics. They have allowed us to recover the probability densities which are solutions of the Schrödinger equation in a direct way, without writing it explicitly. These simulations anticipate the application of scale relativity to turbulence. Indeed, in Lagrangian turbulence experiments,[31,32] one follows Lagrangian small particles which are considered as valid tracers of the fluid elements.[34] In our framework, the trajectories of these tracers can then be considered as concrete manifestations of the virtual fractal geodesics introduced in the scale relativity approach.

In the present paper, we first compare the characteristics of turbulent fluids to the various principles underlying the construction of the scale relativity theory (SRT) (Sec. II). We show in Sec. III how the various physical and mathematical tools of scale relativity are fully supported by experimental data of turbulent flows. We also briefly review the basic mathematical methods by which one constructs the wave function and the geodesics equation, showing that they are well-known and proven methods widely used in stochastic descriptions of turbulence: it is just their special combination which is specific of scale relativity. In Sec. IV, the Schrödinger form of the equation of motion is derived, first in position space and then in velocity space for application to turbulence.[6] Section V describes the main implications and theoretical predictions that one can expect from the new approach, in particular, those which can be experimentally put to the test: the main one is the prediction of the existence of a new acceleration component $A_q = \pm\mathcal{D}_v\, \partial_v \ln P_v$, where $P_v = |\psi_v|^2$ is the local PDF of velocity given by the square of the modulus of a wave function ψ_v, which is solution of a Schrödinger-like equation. We list in Sec. VI some experimental observations and results that already come in support of these theoretical expectations and we end by a discussion and conclusion in Sec. VII.

II. SCALE RELATIVITY DESCRIPTION VS TURBULENCE

The application of the theory of scale relativity[18,19] to turbulence[6] is supported by many elements.[29,35] Indeed, let us recall the various ingredients of this theory and put them in correspondence with some recognized characteristics of turbulent fluids.

- **Scale dependence**. The scale relativity theory (SRT) aims at describing systems which are explicitly dependent on scales. It is well known that this is just the case for a fully developed turbulent fluid.
- **Scale variables**. In SRT, one describes this scale dependence through the introduction of one or several scale variables. For example, a standard time-dependent function $f(t)$ is replaced by a two-variable function $f(t, \delta t)$ depending on time t and time scale δt.

  In turbulent fluids, it is well-known that several physical quantities are explicitly scale dependent in the inertial range, i.e., from the Kolmogorov dissipative small scales to the integral large scales where the energy is injected. For example, in the Lagrangian description in terms of fluid particle trajectories, the accelerations measured for small test-particles are explicitly dependent on the time interval $\tau = \delta t$ (see Fig. 4).[36,32,31,37]
- **Relativity of scales**. The theory of scale relativity relies on the fact that the various scales are not absolute, but only relative. Indeed, only ratios of scales do have a physical meaning, not a scale by itself. This new relativity is therefore expressed in terms of multiplicative groups instead of the usual additive groups of motion relativity. However, the relevant scale variables being actually given by logarithms of scale intervals ratios, e.g., $\ln(\tau/T)$, one recovers standard additive groups in terms of these logarithmic variables.

  The study of turbulent fluid just involves a scale description in terms of such variables, for example, $\ln(\tau/T_L)$ or $\ln(\tau/\tau_\eta)$ in the Lagrangian representation, where T_L is the Lagrangian integral time scale and τ_η is the Kolmogorov dissipative time scale. The scale relativity aspect of turbulence is manifested by the need of such reference scales in the definition of the scale variables since the dimensioned scale interval $\tau = \delta t$ has no meaning in itself, but only the ratio between this scale and the reference scale.
- **Chaotic trajectories**. The application of the scale relativity theory to the macroscopic realm is specific of chaotic systems, at time scales larger than their horizon of predictibility (Ref. 18, Chap. 7.2). On these time scales (larger than about 10 to 20 Lyapunov times), the strict determinism is lost and one is led to use a stochastic description. This ensures the first condition underlying the scale relativity description, according to which there is an infinity (or at least a very large number) of possible trajectories whatever the initial conditions are.

  It is well known that the fluid element trajectories in a turbulent fluid are chaotic.[1] In effect, the predictibility of individual trajectories is lost after some Kolmogorov times (see Fig. 3).
- **Scale laws**. One of the three main conditions upon which the scale relativity description relies is the fractal dimension $D_f = 2$ of trajectories. In position space, it is expressed by the fact that the space increments and the time increments are no longer of the same order since $\delta x \sim \delta t^{1/2}$.

  In a similar way, fractality with dimension $D_f = 2$ in velocity space is expressed by the relation $\delta v \sim \delta t^{1/2}$. This is just the universal Kolmogorov (K41) scaling law in the Lagrangian representation.[4] Recall that it can be obtained by simple dimensional analysis based on the assumption that the various scale dependences be driven by the mere energy ε transferred between scales in the turbulent cascade[5] (which is also the energy finally dissipated into heat at Kolmogorov viscous scales). In the Eulerian representation, one finds $\delta v \sim \delta x^{1/3}$.
- **Irreversibility**. The third condition on which the obtention of a Schrödinger-type equation relies in the theory of scale relativity is local irreversibility. In the new description, velocities are fractal functions, i.e., explicitly scale dependent functions $v(t, \delta t)$. Their derivative (the acceleration) must be defined from two points, the second point being taken after [i.e., from the velocity increment $v(t + \delta t, \delta t) - v(t, \delta t)$] or before the initial point [$v(t, \delta t) - v(t - \delta t, \delta t)$]. There is no *a priori* reason for the two increments to be the same, which leads to a fundamental two-valuedness of the acceleration (that we describe in terms of complex numbers).

  It is widely known that the trajectories of fluid elements in a turbulent fluid are irreversible.[38] Here, this local irreversibility takes a new meaning, when it is accounted for by this doubling of the acceleration vector and combined with the fractality of trajectories in velocity space.
- **Newtonian regime**. As we have recalled, we need the Newtonian dynamics (linking the force to the second derivative of the variable) to obtain a Schrödinger form of the motion equation from fractality and nondifferentiability. A Langevin regime (in which the action of a force is a velocity instead of an acceleration) does not yield this result (Ref. 19, Chap. 10).

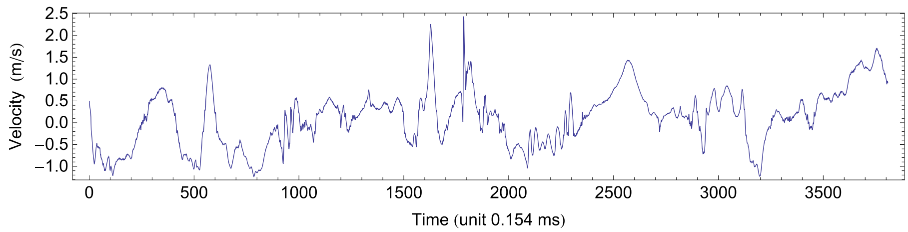

FIG. 1. Example of evolution in a function of time of the velocity of a Lagrangian particle (Seg3398 of Mordant's experiment man290501).

The basic equations of fluid mechanics are the Navier-Stokes equations which are clearly of Newtonian nature (i.e., they involve the second derivative of the variable), even if they contain a dissipative viscous term. The same is true after jumping to velocity space: the basic variable becomes the velocity vector, and the equation of dynamics is just the time derivative of the Navier-Stokes equations.

- **Range of fractal scales**. The last condition is that the range of scales involving a $D_f = 2$ fractal-type behavior be large enough for the relation $\delta v \sim \delta t^{1/2}$ be fulfilled, at least in an effective way (Ref. 19, Sec. 10.3.2).

In turbulent fluids, this means establishing the conditions under which the K41 scaling can be observed. The range of scales where it manifests itself is the inertial range, which is limited by the Kolmogorov dissipative scale τ_η and the integral scale T_L. As recalled in the Introduction, their ratio is given by

$$\frac{T_L}{\tau_\eta} \approx \frac{R_\lambda}{2\,C_0}, \tag{1}$$

i.e., according to the estimated values of $C_0 = 4$–7,[31,39–43] the range of scales is $\approx R_\lambda/10$. The transition to fully developed turbulence is estimated to be at $R_\lambda \approx 500$, yielding a scale ratio 50, while $R_\lambda \approx 1000$ yields $T_L/\tau_\eta \approx 100$, as experimentally observed.[37,32] As we shall see, a well defined (effective) Kolmogorov regime is observed under these conditions (see Fig. 5).

III. EXPERIMENTAL SUPPORT FOR THE APPLICATION OF SRT TO TURBULENCE

A. Infinite number of virtual trajectories

In a turbulent fluid, the trajectories in v-space are no longer deterministic. Namely, under the same initial conditions of velocity and acceleration (v_0, a_0) [and more generally (x_0, v_0, a_0)], the subsequent evolution of a fluid particle is not determined on time scales larger than the Kolmogorov dissipative time scale τ_η. This is supported by all turbulence experiments such as Lagrangian-type experiments where one follows small particles considered to be valid tracers of the fluid particles (see Figs. 1 and 2). In von Karman contra-rotative experiments, it has been shown that particles of size $< \approx 100\ \mu$m achieved such valid tracers.[32]

We have given in Fig. 3 an example of five trajectories in v-space starting from nearby initial conditions in velocities and accelerations. It is clear on the figure that during the first instants (of some τ_η's), there is a memory of the initial conditions and a partial determinism, after which the trajectories diffuse in a Brownian-like chaotic way. This is in agreement with the observed correlation time of an acceleration of $\approx 2.5\tau_\eta$.[37]

This supports a description in terms of stochastic scale-dependent variables, $v = v(t, \delta t)$.

B. Scaling laws

The basic stochastic (and Lagrangian K41) scaling law in the inertial range $\delta v \sim \tau^{1/2}$ (where τ is the time increment, $\tau = \delta t$) or equivalently for accelerations $\sigma_a(\tau) \sim \tau^{-1/2}$ can be shown to be present in an effective way in Lagrangian experimental data of fully developed turbulence ($R_\lambda > \approx 500$); see Fig. 4. As can be seen in Fig. 5, this law is observable locally in individual segments, not only for the full data (3×10^6 velocity values). This is an important point since, as we shall see, the new structures pointed out here, concerning, in particular, the PDF of velocities, are purely local.

As a direct consequence, the expected scaling law for the acceleration a and for its increment da is $a \sim da \sim \delta t^{-1/2}$. This is also confirmed in the experimental data (see Figs. 6 and 7).

C. Time irreversibility and two-valuedness of acceleration

We have plotted in Fig. 6 a comparison between $a(t)$ and its increments $da(t)$ in a function of time for a long trajectory (Seg3398) in Mordant's experiment man290501.[31,37,44,40] The time units are $\tau_u = 0.7$ and $\tau_\eta = 1/6500$ s. The increments da are here simply measured by finite elements $da = a(t_{i+1}) - a(t_i)$ on intervals $t_{i+1} - t_i = \tau_u$.

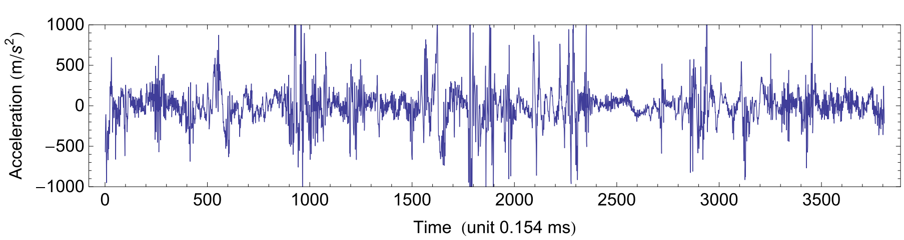

FIG. 2. Time evolution of acceleration for Seg3398 of Mordant's experiment man290501. The intermittency is clearly seen in terms of an alternance of quiet periods followed by bursts of fluctuating very high accelerations.

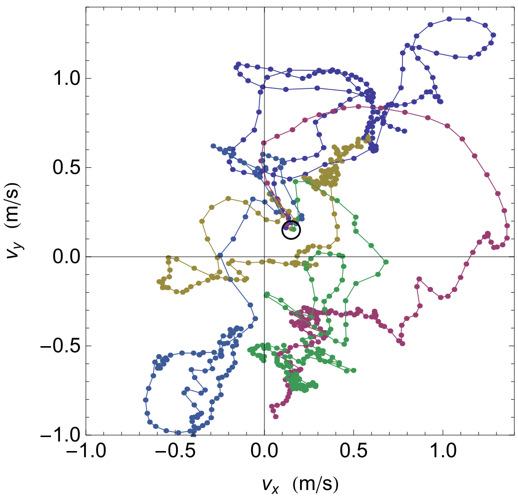

FIG. 3. Example of five 2D trajectories in v-space (from Mordant's[37] 2D experiment) starting from close initial conditions (circle) of velocities ($v_x = v_y = 0.15$ m/s) and accelerations ($a_x = a_y = 300$ m/s^2). Each points are separated by a time interval $\tau_u = 1/6500$ s $\approx 0.7\ \tau_\eta$. The trajectories are followed on a total time 146 $\tau_u = T_L$.

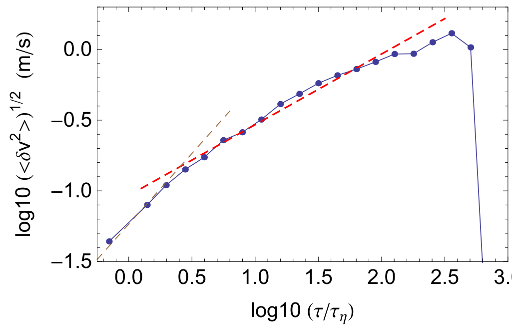

FIG. 5. Time scale dependence of velocity increments in the long segment Seg3398 (3808 velocity values at measurement intervals $\tau_u = 1/6500$ s $\approx 0.7\ \tau_\eta$) of Mordant's experiment man290501 (points), compared with the K41 law $\delta v \sim \delta t^{1/2}$ (red dashed line). The small time scale transition is larger than τ_η due to the too large particle diameter 250 μm. However, the K41 law is achieved in an effective although approximate way on almost two decades.

Two remarkable features appear in this figure.

(i) While for a standard differentiable curve, one would expect $da \ll a$, which is the basis for using the usual differential calculus, it is very clear that this condition is far from being achieved. On the contrary, da is clearly of the same order than a itself, $da \approx a$, and it can therefore not be treated as a standard differential element.

(ii) Moreover, $|a|$ and $|da|$ are not only of the same order, but remarkably similar. Such a possibility has been theoretically anticipated at the beginning of the 1990s:[18] we had found fractal functions whose derivative were quite similar to the function itself (Fig. 8). Strictly, such functions $\xi(x, dx)$ are not differentiable and their derivatives are infinite in the limit $dx \to 0$, but by defining them as explicit functions of the increment dx, a renormalized derivative $d\xi/dx$ can be defined which is now finite and which, in the case considered, looks closely like the initial function ξ. It appears that the time evolution of the acceleration on a particle trajectory in a fully developed turbulent fluid achieves such a predicted behavior in a laboratory experiment.

Such a behavior perturbs in an essential way the standard differential calculus. Let us show that it is profoundly linked to irreversibility and that it involves a two-valuedness of the acceleration field. In the standard nonfractal case, one identifies the acceleration $a = dv/dt$ with the first derivative $v'(t)$. This is clear from performing

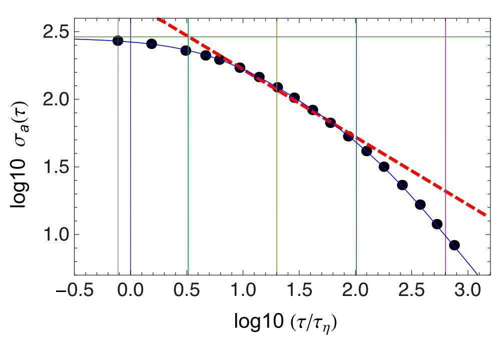

FIG. 4. Time scale dependence of acceleration in Mordant's experiment man290501 (points, $R_\lambda = 800$), compared with a K41 scaling law $\sigma_a(\tau) \sim \tau^{-1/2}$ (red dashed line).The small scale transition is the transition between the inertial (K41) regime and the Kolmogorov dissipative scale τ_η; the value at which the inertial regime is reached is somewhat large in these data ($\approx 5\tau_\eta$) as a consequence of the particle size (250 μm). At large scales, the transition is around the integral time scale T_L, which is ≈ 100 times τ_η in these data.

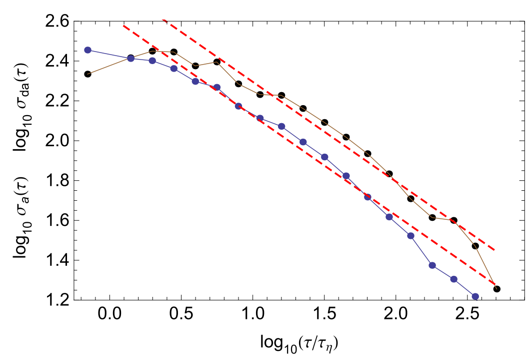

FIG. 6. Time scale dependence of accelerations standard deviations $\sigma_a = \langle a^2 \rangle^{1/2}$ (blue lower points) and acceleration increment standard deviations $\sigma_{da} = \langle da^2 \rangle^{1/2}$ (black upper points) in the long segment Seg3398 (3808 velocity values at measurement intervals $\tau_u = 1/6500$ s $\approx 0.7\ \tau_\eta$) of Mordant's experiment man290501. They are compared with a K41 law $\sim\delta t^{-1/2}$ (red dashed lines). In the inertial range, the amplitude ratio between the two laws is just $\sqrt{2}$ as expected since a is uncorrelated beyond a few τ_η's.[40,44]

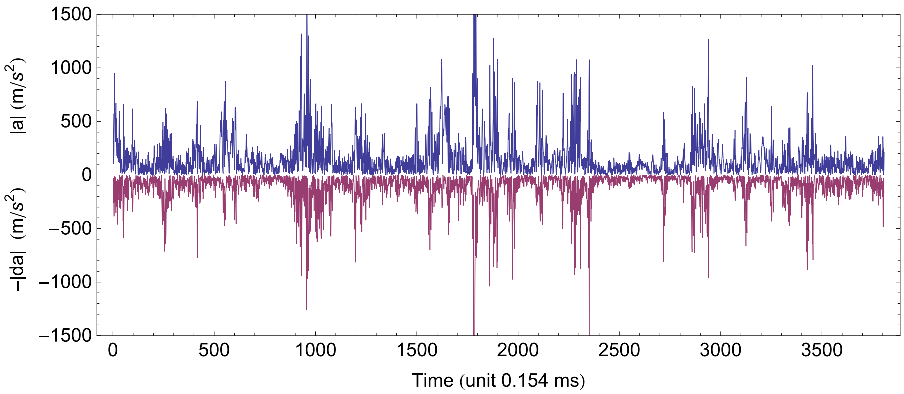

FIG. 7. Variation with time of the acceleration $a(t)$ (absolute value, upper part of the figure) compared to its increment $da(t)$ (absolute value, lower part) for Seg3398 (3808 velocity values at measurement intervals τ_u = 1/6500 s ≈ 0.7 τ_η) of Mordant's experiment #3 man290501.[37,40] The acceleration "differential elements" da are of the same order as a itself, in contradiction with the standard differential calculus which assumes $|da| \ll |a|$.

a Taylor expansion,

$$\begin{aligned}\frac{dv}{dt} &= \frac{v(t+dt)-v(t)}{dt}\\ &= \frac{[v(t)+v'(t)dt+\frac{1}{2}v''(t)dt^2+\ldots]-v(t)}{dt},\end{aligned} \tag{2}$$

so that one obtains

$$\frac{dv}{dt} = v'(t)+\frac{1}{2}v''(t)\,dt+\ldots = v'(t)+\frac{1}{2}dv'(t)+\ldots. \tag{3}$$

For a standard nonfractal function, the contribution $\frac{1}{2}dv'(t)$ and all the following terms of higher order vanish when $dt \to 0$ so that one recovers the usual result $a(t) = dv(t)/dt = v'(t)$. In practice, one does not really take the limit $dt \to 0$, but one considers small time intervals such that $dv' \ll v'$, allowing the same identification (of a and v') in an effective way.

In a fully developed turbulent fluid, we have seen that $da \approx a$ so that $dv' \approx v'$ and the term $\frac{1}{2}dv'(t)$ can no longer be neglected with respect to $v'(t)$. Now, the derivative of $v(t)$ involves two points by definition, which may be chosen to be *after* (at time $t + dt$, for $dt > 0$) or *before* the point $v(t)$ (at time $t - dt$). In the standard differentiable case, the two definitions, $\lim_{dt\to 0}[v(t+dt)-v(t)]/dt$ and $\lim_{dt\to 0}[v(t)-v(t-dt)]/dt$, coincide.

In the nondifferentiable case (and for experimental turbulence), the various quantities become explicit functions of the scale interval dt, which is no longer considered as tending to 0, but as being variable. The Lagrangian velocity can be described by a fractal function $v(t, dt)$, which an explicit function of two independent variables, time t and the (now nonvanishing) differential element dt. Then, the derivative of velocity can take the following two forms:

$$\begin{aligned}\frac{d_+}{dt}\,v(t,dt) &= \frac{v(t+dt,dt)-v(t,dt)}{dt},\\ \frac{d_-}{dt}\,v(t,dt) &= \frac{v(t,dt)-v(t-dt,dt)}{dt}.\end{aligned} \tag{4}$$

The fact that the increment $dv'(t, dt)$ is no longer negligible with respect to the first derivative $v'(t, dt)$ implies that the two possible expressions for the acceleration are no longer equal,

$$\begin{aligned}a_+ &= \frac{d_+}{dt}v(t,dt) = v'(t,dt)+\frac{1}{2}\,dv'(t,dt),\\ a_- &= \frac{d_-}{dt}v(t,dt) = v'(t,dt)-\frac{1}{2}\,dv'(t,dt).\end{aligned} \tag{5}$$

Therefore, there is a two-valuedness of the possible values of the acceleration since, in general, $a_+ \neq a_-$. Note that this two-valuedness does not come from time reversal. The two (+) and (−) values are *not* a forward and a backward acceleration. In both cases, time goes, as physically expected, from past to future: one goes from one definition to the other by the transformation $(dt \to -dt)$, not $(t \to -t)$. Nor is it a left and right derivative of a standard function: this two-valuedness is specific of fractal functions which are explicitly dependent on the finite differential element dt, identified with a resolution interval.

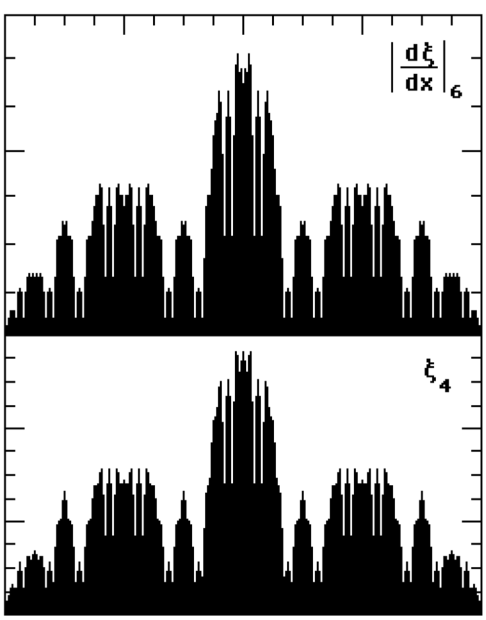

FIG. 8. An example, excerpt from Nottale (1993) (Ref. 18, Fig. 3.18 p. 79), of a fractal function which closely looks like its own derivative. It is constructed from a projection of a fractal curve whose generator is a zig-zag made of 8 segments of length 1/4 (then of fractal dimension D_f = 3/2).

D. Methods

The methods by which these various conditions are mathematically implemented in the theory of scale relativity are actually standard, widely used, methods, in particular, in the domain of turbulence studies (stochastic calculus, Ito formulas, fractals and mutifractals, complex numbers). The new ingredient that leads to original results (namely, a Schrödinger form for the derivative of Navier-Stokes equations after integration) is just their combination, which has not been considered up to now in this form in fluid mechanics.

The infinity of the number of possible trajectories naturally leads to a stochastic description. The use of stochastic differential equations (SDEs) is a standard method in turbulence studies[45–47] and is also a basis of the present approach.

The Ito calculus is particularly adapted to derivation and integration of stochastic variables when second order differential elements intervene in an explicit way. This is just the case for fluctuations in turbulence characterized in the inertial range by different orders for the velocity and time differential elements, according to Kolmogorov scaling $\delta v^2 \sim \delta t$. It is a standard tool in turbulence studies. We also naturally use it to build the "covariant" total derivative which generalizes the Euler derivative $d/dt = \partial/\partial t + v\,\nabla$ (which is specific of fluid mechanics) to fractal geometry.

Fractals and multifractals are now standard tools for building models in the study of turbulence. Here, we use this concept in a somewhat different way since we consider the turbulent fluid as a medium which is fractal in velocity-space and plays the role of a fractal space for the particles moving into it.[18]

Complex numbers are used in the theory of scale relativity as a natural description of the algebra doubling imposed by the two-valuedness of accelerations. We combine the (+) and (−) accelerations in terms of a doublet (a_+, a_-) and then in terms of complex numbers $\mathcal{A} = (a_+ + a_-)/2 - i(a_+ - a_-)/2$.

IV. SCHRÖDINGER FORM FOR THE MOTION EQUATION

A. General argument

As we shall recall hereafter, the combination of the three conditions (infinite number of possible trajectories, scaling law of fractal dimension 2, and local irreversibility) leads to give to the energy equation (integral of a Newtonian equation of dynamics) a Schrödinger-type form.[18] This result is obtained from a general mathematical argument, which does not depend on the nature of the variables. We shall first remind how it is obtained in position space as made in previous publications whose goal was to describe the dynamics in a fractal space.[19] This case corresponds to a fundamental fractality relation $\delta x \sim \delta t^{1/2}$ which characterizes paths of fractal dimension 2 (as expected for stochastic Markovian paths being neither correlated nor anticorrelated).

However, in the case of laboratory turbulence, as pointed out by Montera,[6] the fractality is not in position space but in velocity space, as shown by the Lagrangian K41 scaling relation $\delta v \sim \delta t^{1/2}$. He then made the remarkable suggestion of applying the scale relativity theory to turbulence in v-space instead of x-space. In other words, the fundamental space variable becomes the velocity v, and the equivalent of the successive derivatives (x, v, a) become $(v, a, \dot{a})$.

Therefore, the Navier-Stokes equation remains unaffected by this new dynamics, but its derivative takes, after integration, the form of a Schrödinger-type equation.

B. Scale relativity theory in position space: A short reminder

The laws of motion are obtained in the scale relativity theory by writing the fundamental equation of dynamics (which reduces to a geodesic equation in the absence of an exterior field) in a fractal space (more generally, space-time). As we have seen, the nondifferentiability and the fractality of coordinates implies at least three consequences:[18,19]

(1) The number of possible paths is infinite. The description therefore naturally becomes nondeterministic and probabilistic. These virtual paths are identified with the geodesics of the fractal space. The ensemble of these paths constitutes a fluid of geodesics, which is therefore characterized, as a first step, by a velocity field $V(X, t)$ in the Eulerian representation. The individual geodesics, which describe the possible trajectories of particles and are therefore of Lagrangian essence, are linked to this Eulerian field by the relation $dX_\alpha/dt = V[X_\alpha(t), t]$, for each geodesic labeled by α.

(2) Each of these paths is itself fractal with dimension 2. The velocity field is therefore a fractal function, $V(x, t, dt)$, explicitly dependent on resolutions and divergent when the scale interval tends to zero (this divergence is the manifestation of nondifferentiability).

(3) Moreover, the nondifferentiability also implies a two-valuedness of this fractal function, $\{V_+(X, t, dt), V_-(X, t, dt)\}$. Indeed, two definitions of the velocity field now exist, which are no longer invariant under a transformation $|dt| \to -|dt|$ in the nondifferentiable case. These three properties of motion in a fractal space lead to describing the geodesic velocity field in terms of a complex fractal function,

$$\mathcal{V} = \frac{V_+ + V_-}{2} - i\,\frac{V_+ - V_-}{2}. \tag{6}$$

The elementary displacements along these geodesics can be described in terms of stochastic differential equations (SDEs), decomposing them as the sum of a mean and a fluctuation. They take two forms which read (in Lagrangian representation)

$$dX_+ = v_+\, dt + d\xi_+, \tag{7}$$

$$dX_- = v_-\, dt + d\xi_-. \tag{8}$$

The scale dependence of the fractal fluctuations reads $d\xi_\pm = \zeta_\pm \sqrt{2\mathcal{D}}\,|dt|^{1/2}$, with $\zeta_\pm$ being a dimensionless stochastic variable such that $\langle \zeta_\pm \rangle = 0$ and $\langle \zeta_\pm^2 \rangle = 1$. The parameter $\mathcal{D}$ characterizes their amplitude.

Using Ito calculus, these various effects can be combined in terms of a total derivative operator[18] which generalizes to fractal geometry the Euler total derivative (and therefore applies to the Eulerian representation),

$$\frac{\widehat{d}}{dt} = \frac{\partial}{\partial t} + \mathcal{V}.\nabla - i\mathcal{D}\Delta. \tag{9}$$

Various equivalent representations of the equations of dynamics become now possible by using this tool.

1. Geodesic representation

The first representation, which can be considered as the root representation, is the geodesic one. The two-valuedness of the velocity field is expressed in this case in terms of the complex velocity field $\mathbb{V} = V - iU$. It implements what makes the essence of the principle of relativity: namely, the equation of motion, once written in terms of the covariant derivative Eq. (9), takes the form of a free inertial equation devoid of any force

$$\frac{\widehat{d}}{dt}\mathcal{V} = 0, \tag{10}$$

where the "covariant" derivative operator $\widehat{d}/dt$ includes the terms which account for the effects of the geometry of space—more generally of space-time in the "relativistic" case (see Ref. 19 and references therein). In the presence of an exterior potential, the equation of dynamics takes Newton's form

$$m\,\frac{\widehat{d}}{dt}\mathcal{V} = -\nabla\phi. \tag{11}$$

2. Schrödinger representation

A wave function ψ can be introduced[18] as a re-expression of the action $\mathcal{S} = -2i\mathcal{D}\ln\psi$ (which is now complex since the velocity is complex). As a consequence of the fundamental canonical relation $\mathcal{P} = m\mathcal{V} = \nabla\mathcal{S}$, the velocity field of geodesics is related to the wave function according to

$$\mathcal{V} = -2i\mathcal{D}\,\nabla\ln\psi. \tag{12}$$

This means that the two-valuedness of the velocity field (coming from nondifferentiability) is expressed in terms of two quantities, the squared modulus P and the phase θ of this wave function.

By replacing the complex velocity in Eq. (11) by this expression, one finds that the equation of motion can be integrated under the form of a Schrödinger equation,[18]

$$\mathcal{D}^2\Delta\psi + i\,\mathcal{D}\frac{\partial}{\partial t}\psi - \frac{\phi}{2m}\,\psi = 0. \tag{13}$$

3. Fluid representation with quantum potential

By decomposing the complex wave function $\psi = \sqrt{P} \times e^{i\theta/2\mathcal{D}}$ in terms of a modulus $\sqrt{P}$ and a phase $\theta/2\mathcal{D}$ (related to the real part of the velocity field by the relation $V = \nabla\theta$), one can give this equation the form of hydrodynamics equations including a quantum potential.[18,48,19,49]

Indeed, the imaginary part of the Schrödinger equation becomes a continuity equation,

$$\frac{\partial P}{\partial t} + \mathrm{div}(PV) = 0. \tag{14}$$

The real part takes the form of an Euler equation,

$$m\left(\frac{\partial}{\partial t} + V.\nabla\right)V = -\nabla(\phi + Q), \tag{15}$$

where Q is an additional potential energy that depends on the probability density P,

$$Q = -2m\mathcal{D}^2\,\frac{\Delta\sqrt{P}}{\sqrt{P}}. \tag{16}$$

The additional quantum potential is obtained here as a direct manifestation of the fractal geometry of space, in analogy with Newton's potential emerging as a manifestation of the curved geometry of space-time in Einstein's relativistic theory of gravitation.

C. Velocity space: Application to laboratory turbulence

The application of the scale relativity approach to fluid turbulence in the inertial range (where the relation $\delta v \sim \delta t^{1/2}$ strictly holds) amounts to just shift the variables (x, v, a) to $(v, a, \dot{a})$. Now, the velocity V is the primary variable, while the fundamental local irreversibility leads to a two-valuedness of the acceleration field, (A_+, A_-), which is represented in terms of a complex acceleration,

$$\mathcal{A} = \frac{A_+ + A_-}{2} - i\,\frac{A_+ - A_-}{2} = A_R - iA_I. \tag{17}$$

In the inertial range and neglecting for the moment the Langevin term $-v/T_L$, the new Lagrangian description starts with two stochastic differential equations in v-space,

$$dV_+ = A_+\,dt + dV_{\xi+}, \tag{18}$$

$$dV_- = A_-\,dt + dV_{\xi-}, \tag{19}$$

where the scale dependence of the stochastic fluctuation reads, in agreement with the K41 scaling law,

$$dV_{\xi\pm} = \zeta_\pm\,\sqrt{2\mathcal{D}_v}\,|dt|^{1/2}. \tag{20}$$

Such linear SDEs are known to yield Gaussian processes (see Ref. 47 and references therein). Therefore, the reduced variable $\zeta_\pm$ is taken here to be a dimensionless Gaussian stochastic variable such that $\langle\zeta_\pm\rangle = 0$ and $\langle\zeta_\pm^2\rangle = 1$. The parameter $\mathcal{D}_v$ characterizes the amplitude of the fluctuations.

Using the Ito calculus, these various effects can be combined in terms of a total derivative operator acting in v-space,

$$\frac{\widehat{d}}{dt} = \frac{\partial}{\partial t} + \mathcal{A}\cdot\nabla_v - i\,\mathcal{D}_v\Delta_v. \tag{21}$$

The Navier-Stokes equation (reduced to the Euler equation in the inertial range by neglecting for the moment the viscous term) writes in Lagrangian form $dv/dt = F$. Its derivative with respect to time reads

$$\frac{da}{dt} = \dot{F}. \tag{22}$$

In order to account for the various effects described here, one replaces d/dt by the new total derivative operator $\widehat{d}/dt$, which includes the effects of fractality and nondifferentiability. One obtains the new equation

$$\frac{\widehat{d}}{dt}\mathcal{A} = \left(\frac{\partial}{\partial t} + \mathcal{A}\cdot\nabla_v - i\,\mathcal{D}_v\Delta_v\right)\mathcal{A} = \dot{F}. \tag{23}$$

Let us now consider in more detail the right-hand side of this equation, which is a "force" in v-space, that we can formally write $\dot{F}(v)$. We shall show that, in the case of a turbulent fluid as considered here, this v-force is expected to derive from a potential, $\dot{F}(v) = -\nabla_v \Phi_v(v)$. Indeed, it is well known that a fully developed turbulent fluid can be decomposed in terms of a cascade of eddies. The pulsating[5] or oscillatory nature of the motion in eddies naturally leads us to formalize it (at a given instant and for each variable), as resulting from a sum of oscillators,

$$\frac{dv}{dt} = -\sum_k \nabla_x \left(\frac{1}{2}\, \omega_k^2 \,(x - x_k)^2 \right). \tag{24}$$

The force then derives from an oscillator potential in x-space. The nature of oscillators is such that the same will be true in v-space, i.e., one can write

$$\frac{da}{dt} = -\sum_k \nabla_v \left(\frac{1}{2}\, \omega_k^2 \,(v - v_k)^2 \right), \tag{25}$$

where ω_k's and v_k's are functions of time. One can add to these harmonic oscillator terms of damping or forcing and more generally make them anharmonic. In all cases, the main part of the force derives from a potential, in position space (as known from the Navier-Stokes force $-\nabla_x p/\rho$), but also in velocity space. This remark becomes particularly useful with the Schrödinger form of the motion equation that we shall obtain since oscillator solutions (harmonic and anharmonic) are well known and largely studied in standard quantum mechanics.

Therefore, a leading contribution to the total force can be written in terms of the v-gradient of a potential Φ_v, and, now including the contributions from fractality and nondifferentiability, we get the equation

$$\frac{\widehat{d}}{dt} \mathcal{A} = -\nabla_v \Phi_v. \tag{26}$$

This equation of dynamics in v-space is just the Euler-Lagrange equation written from a Lagrange function $L_v = L_v(v, \mathcal{A}, t)$, which is now complex since the acceleration $\mathcal{A}$ is complex. As a direct consequence, the action in v-space $\mathcal{S}_v = \sum L_v dt$ is also complex. It is linked to the acceleration by the canonical relation $\mathcal{A} = \nabla_v \mathcal{S}_v$, and it can be re-expressed in terms of a complex "wave function" ψ_v following the relation:

$$\mathcal{S}_v = -2i\mathcal{D}_v \ln \psi_v. \tag{27}$$

This wave function can be decomposed in terms of a modulus and a phase

$$\psi_v = \sqrt{P_v} \times e^{i\theta_v/2\mathcal{D}_v}. \tag{28}$$

The main point here is that the PDF of velocities is given by the square of the modulus of the wave function, $P_v(v) = |\psi_v|^2$, while its phase is linked to the real part of the complex acceleration through the relation $A_R = \nabla_v \theta_v$. The constant $2\mathcal{D}_v$ is therefore the macroscopic equivalent in v-space of the constant $\hbar$ of standard quantum mechanics (for $m = 1$).

Finally, the derivative of the fluid equations takes, after integration, the form of a macroscopic Schrödinger equation[6,35,29]

$$\mathcal{D}_v^2 \,\Delta\psi_v + i\,\mathcal{D}_v \frac{\partial}{\partial t}\psi_v - \frac{\Phi_v}{2}\,\psi_v = 0. \tag{29}$$

This Schrödinger equation describes the effects of the part of the turbulent force which can be written in terms of the gradient of a potential in v-space. As we have argued, the proven existence of eddies, which we describe as oscillators, supports the conclusion that this part is dominant, at least in the inertial range. However, the very construction of this Schrödinger equation relies on the cascade through the relation $\delta v^2 \sim \delta t$. Therefore, we expect the potential Φ_v to be mainly given by the largest eddies at the large scale end of the inertial range. As we shall see, the experimental laboratory data fairly support this conclusion.

Moreover, since it concerns only the inertial range, this Schrödinger equation does not contain all the contributions to the dynamics, but it can be considered as a kind of kernel to which other effects (nonpotential terms, Langevin term, viscosity, etc.) can be added (see Ref. 48).

As a consequence of the standard relation of Lagrange mechanics (here in v-space), $\mathcal{A} = \nabla_v S_v$, the complex acceleration writes, in terms of the wave function,

$$\mathcal{A} = -2i\,\mathcal{D}_v\,\nabla_v \ln \psi_v \tag{30}$$

so that we are now able to establish the expression for the two new acceleration components A_+ and A_-,

$$A_+ = +\mathcal{D}_v\,\frac{\partial_v P_v}{P_v} + \partial_v \theta_v, \tag{31}$$

$$A_- = -\mathcal{D}_v\,\frac{\partial_v P_v}{P_v} + \partial_v \theta_v. \tag{32}$$

In many situations which may be relevant to the turbulence case, in particular, for a harmonic oscillator potential expected to describe the largest eddies of the turbulent cascade as a first approximation, the solutions of the Schrödinger equation are real,[50] i.e., $\theta_v \approx$ cst and then $\partial_v \theta_v \approx 0$. Under this approximation (which is supported by the experimental data), the new acceleration can then be written as

$$A_q = \pm\mathcal{D}_v\,\frac{\partial_v P_v}{P_v}. \tag{33}$$

The SDEs which describe the possible trajectories of fluid particles then write

$$dV_\pm = -\frac{V}{T_L}\,dt \pm \mathcal{D}_v\,(\partial_v \ln P_v)\,dt + dV_{\xi\pm}, \quad \langle dV_{\xi\pm}^2(\tau)\rangle = 2\mathcal{D}_v \tau, \tag{34}$$

where $\tau = \delta t$ is a varying time scale interval and $\mathcal{D}_v$ is a constant diffusion coefficient in v-space. We have added a Langevin large scale contribution in order to account for the velocity autocorrelation and to connect our approach to the SDE usually written in stochastic models of turbulence,[45–47]

$$dV = -\frac{V}{T_L}\,dt + dW_\xi, \quad \langle dW_\xi^2(\tau)\rangle = 2D_0\tau. \tag{35}$$

There are some important differences between the two models:

(i) The new contribution A_q is expected to now carry a large part of the acceleration variance. As we shall see in what follows, this is supported by experimental data: we find that about 85% of the variance is accounted by A_q alone. Therefore, the diffusion coefficient in the new model is expected to be smaller than in the standard one, $\mathcal{D}_v \ll D_0$;

(ii) There are two SDEs instead of one because of the two-valuedness ± (but they can be combined in terms of a single complex SDE);

(iii) If one wants to account for intermittency and highly non-Gaussian large tails of the acceleration PDF from the usual SDE, one should introduce a non-Gaussian probability distribution of the stochastic fluctuation. In this framework, the very origin of this non-Gaussianity is still unknown even though it can be described by multifractal models[9,1,10–12] or by making the model coefficients themselves stochastic processes.[51] In the new scale relativity framework, we shall show that the wide tails of the acceleration PDF can be obtained as an effect of the new acceleration component A_q **alone** (see Sec. VI D). The stochastic fluctuation has therefore no reason to remain non-Gaussian and can be described by a simple Brownian motion in v-space. As we shall see in the following, this is supported by experimental data, since we find that the calm periods of the intermittent acceleration, which are just the zones where $A_q \approx 0$, i.e., of pure fluctuations are perfectly Gaussian (see Sec. VI E and Fig. 21).

Finally, the full process in the scale relativity approach to turbulence is described by a combination of two coupled equations, for $A_\pm$ a SDE, and for the derivative of $A_\pm$ the Schrödinger equation (which is just an expression of the derivative of the Navier-Stokes equation written in fractal v-space, $\widehat{d}\mathcal{A}/dt = -\nabla_v \Phi_v$, in the inertial domain)

$$A_\pm = -\frac{V}{T_L} \pm \mathcal{D}_v\,(\partial_v \ln P_v) + A_{\xi\pm}, \quad \langle A^2_{\xi\pm}(\tau)\rangle = 2\mathcal{D}_v/\tau, \tag{36}$$

$$\mathcal{D}_v^2\,\Delta\psi_v + i\,\mathcal{D}_v \frac{\partial}{\partial t}\psi_v - \frac{\Phi_v}{2}\,\psi_v = 0, \quad P_v = |\psi_v|^2, \tag{37}$$

where $A_{\xi\pm}$ is the time derivative of the stochastic process $dV_{\xi\pm}$. We shall give, in what follows, examples of numerical simulations of solutions to these coupled equations.

This system can be put in correspondence with some standard stochastic approaches, in which, instead of a mere Langevin SDE, two-level equations [an ordinary differential equation (ODE) for the acceleration a and an SDE for its derivative $\dot{a}$] are also used.[52,45,47]

1. Quantum-classical transition

One of the main features of standard quantum mechanics is the existence of a quantum to classical transition around the de Broglie length-scale. A system becomes quantum for length-scales smaller than $\lambda_{dB} = \hbar/(m\langle v^2\rangle^{1/2}) = \hbar/m\sigma_v$ and classical at larger scales.

The equivalent transition in the case of fluid turbulence is naturally a velocity-scale, $\delta v_{dB} = \hbar_v/\langle a^2\rangle^{1/2} = \hbar_v/\sigma_a = 2\mathcal{D}_v/\sigma_a$, where $\sigma_a = \langle a^2\rangle$ is the standard deviation of acceleration. The role of the Planck constant $\hbar_v$, here defined in v-space, is now played by the constant $2\mathcal{D}_v$ (for $m = 1$).

However, the existence of a lower time scale, the Kolmogorov dissipative scale τ_η, transforms this velocity interval into an acceleration $a_{dB} = \delta v_{dB}/\tau_\eta$. We know that, under the K41 regime, the acceleration variance is given by[53,54]

$$\sigma_a^2 = A_0 \frac{\varepsilon}{\tau_\eta}, \tag{38}$$

where A_0 is a numerical constant which has been estimated to be, in fully developed turbulence ($R_\lambda > \approx 500$), $A_0 \approx 4$ in DNS and $A_0 \approx 6$ from experimental data.[32] It is smaller in the work of Mordant *et al.* data,[40] $A_0 \approx 1$, probably due to the too large particle size.[34] We also know that, in the K41 regime,

$$2D_0 = C_0\,\varepsilon = \frac{2\,\sigma_v^2}{T_L}. \tag{39}$$

Then, we find from these various relations that the de Broglie-like acceleration transition is given by

$$a_{dB} = \frac{\mathcal{D}_v}{D_0}\frac{C_0}{A_0}\,\sigma_a \approx \sigma_a. \tag{40}$$

Therefore, we expect macroscopic quantumlike effects to manifest at accelerations $a < \approx\sigma_a$, while the large accelerations remain "classical." As we shall see, experimental data support this expectation (see Figs. 10 and 13).

V. IMPLICATIONS AND THEORETICAL PREDICTIONS

The main implications of this new approach that one can theoretically predict are as follows:

- The velocity PDF is expected to be locally given by the square of the modulus of a complex "wave function," $P_v = |\psi_v|^2$.
- The function ψ_v is a solution of a Schrödinger-type equation. It can have any sign and is generally expected to jump from one sign to the other at some values v_i.
- We therefore expect the occurrence of specific values v_i of the velocity v, defined as those for which $P_v(v_i) = 0$. In most cases, one expects $\psi_v(v) \propto \pm(v - v_i)$ around these values so that $P_v(v) \propto (v - v_i)^2$. A typical example of this behavior is given by harmonic oscillator solutions of the Schrödinger equation (see Fig. 9).
- The new acceleration component $A_q = \pm\mathcal{D}_v\,(\partial_v P_v)/P_v$ becomes clearly divergent around the values where $P(v_i) = 0$, i.e., $A_q \to \pm\infty$ when $v \to v_i$ (Fig. 9). We have suggested[29] that these divergences are the cause for the large tails of the acceleration PDF in a turbulent fluid. We shall show in the following (Sec. VI D) that experimental laboratory data[32,7,37,44] can be precisely fitted by the analytical PDF deduced from the expression of A_q (see Fig. 20).
- Intermittent bursts of acceleration. From this process, we expect the particle to alternate between being confined in the probability peaks of the velocity PDF (where P_v is large and therefore A_q is small) and jumping from one peak to another, thus crossing the values v_i involving bursts of very large accelerations (see Fig. 13). Such an alternation between calm periods and bursts of large accelerations is specifically the process of intermittency, which is typical of turbulence.
- Calm zones of acceleration. Since the large tails of the acceleration PDF are now accounted for by the new acceleration component A_q, the residual stochastic fluctuation is now Gaussian in our model. Therefore, we expect the calm intermittent periods, which correspond to $A_q \approx 0$ and are given by

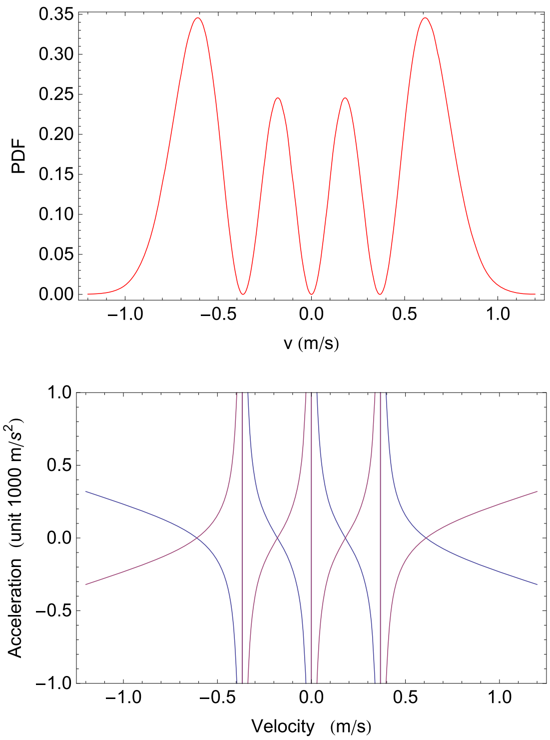

FIG. 9. Top figure: PDF of velocity for a macroquantum harmonic oscillator, in the excited state $n = 3$, for $v_0 = 0.3$ m/s. Down figure: typical shapes of the accelerations $A_q(v) = \pm D_v\ \partial_v \ln P_v$, expected for the PDF of velocity $P_v(v)$ given in the top figure. The acceleration becomes divergent on the null minima of the velocity PDF (see top figure).

the mere stochastic background fluctuation, to be Gaussian. This is remarkably confirmed by analysis of experimental data (see Fig. 21).

- Numerical simulations. Some analytical results can be obtained from the mere expression of A_q, such as the PDF of acceleration (see Ref. 29 and the following Sec. VI D). One can extend the analysis by performing numerical simulations integrating the system of Eq. (37) [this is similar to previous simulations performed in x-space in the context of standard quantum mechanics[33] (Ref. 19, Chap. 10.5)]. These simulations are used, in particular, to deduce from the Schrödinger/A_q process the expected correlation function of the acceleration modulus (see Figs. 22 and 23) and the exponents of structure functions (Fig. 25), which are in good agreement with the experimentally observed ones.

VI. EXPERIMENTAL VALIDATIONS OF THEORETICAL PREDICTIONS

The theoretical predictions of the scale relativity approach to turbulence listed here above can be checked in specific and possibly dedicated experiments. These predictions rely on a Schrödinger-type velocity PDF which is stable on time scales larger than the correlation time T_L. This is because the large eddy oscillator potential which drives the solutions of the Schrödinger equation remains itself stationary on larger times. The identification of such PDFs can be deduced from data analysis of the histograms of observed velocities, and it therefore requires the obtention of long enough Lagrangian trajectories ($\gg T_L$) individually analyzed, moreover sampled at times-scales equal or smaller than the Kolmogorov time τ_η. These kinds of data are very rare since most experiments have privileged global statistics on a high number of short trajectories. The acoustic Doppler velocity measurements of N. Mordant in 2001[37] in contra-rotative turbulent flows have provided data on Lagrangian trajectories of length up to 26 T_L sampled under τ_η, which is therefore relevant for our purpose. We shall mainly focus in what follows on data analysis of these experiments.

We shall now review the main experimental validations and proofs of the theoretical predictions made in this new model of turbulence, by giving some typical examples from analysis of experimental data. Note that the general argument given in Sec. IV C is valid for both compressible and incompressible flows. However, in the present paper, we consider experimental validations from data obtained with only incompressible fluids. The compressible case will be studied in more detail in forthcoming works.

A. Empty zones and non-Gaussianity of local velocity PDF

It is well known that the local velocity PDF (i.e., that of individual Lagrangian trajectories) is far from Gaussian (see, e.g., Figs. 10 and 13).

Some examples of experimental (v, a) "phase" diagrams are given in Fig. 10. They very clearly support the systematic existence of empty zones in the "local" velocity PDF. We call here "local" the PDF derived from one unique Lagrangian trajectory or trajectory segment of a particle (which is a valid tracer of the flow) instead of the PDF of the full Lagrangian field constructed from adding the data from a large number of different segments. Indeed, this mixing of different trajectories would smooth out the Schrödinger-type structures that we expect to be manifested since the oscillator potential in the Schrödinger equation is given by a large scale eddy which is expected to evolve with time and/or to jump to a different one.

Note also that these structures appear only for $a < \approx\sigma_a$, as expected from the existence of a "macroquantum"-classical transition around $a = \sigma_a$ (Sec. IV C). Then, the values of the zero minima v_i of P_v change from one segment to the other. Therefore, they are not observable through the usual method of analysis, which consists of accumulating a large number of velocity values (e.g., 3×10^6 in Mordant's experiment man290501,[37,40] more than 10^8 in some recent experiments[7]). Such a sum will clearly destroy the minima by phase mixing (see Fig. 10) and lead to a final strict Gaussian distribution as expected from the central limit theorem and as experimentally observed.[31,32]

B. Direct validation of the new acceleration component A_q

The new acceleration contribution $A_q = \pm\mathcal{D}_v\ \partial_v \ln P_v^q(v)$, where $P_v^q(v)$ is the velocity PDF for $|a| < \sigma_a$, can be directly obtained from the local velocity PDF $P_v^q(v)$. This PDF can be established from a histogram of velocities on a given trajectory. The values of A_q depends on the distance of v to the nearest zero minimum v_i of

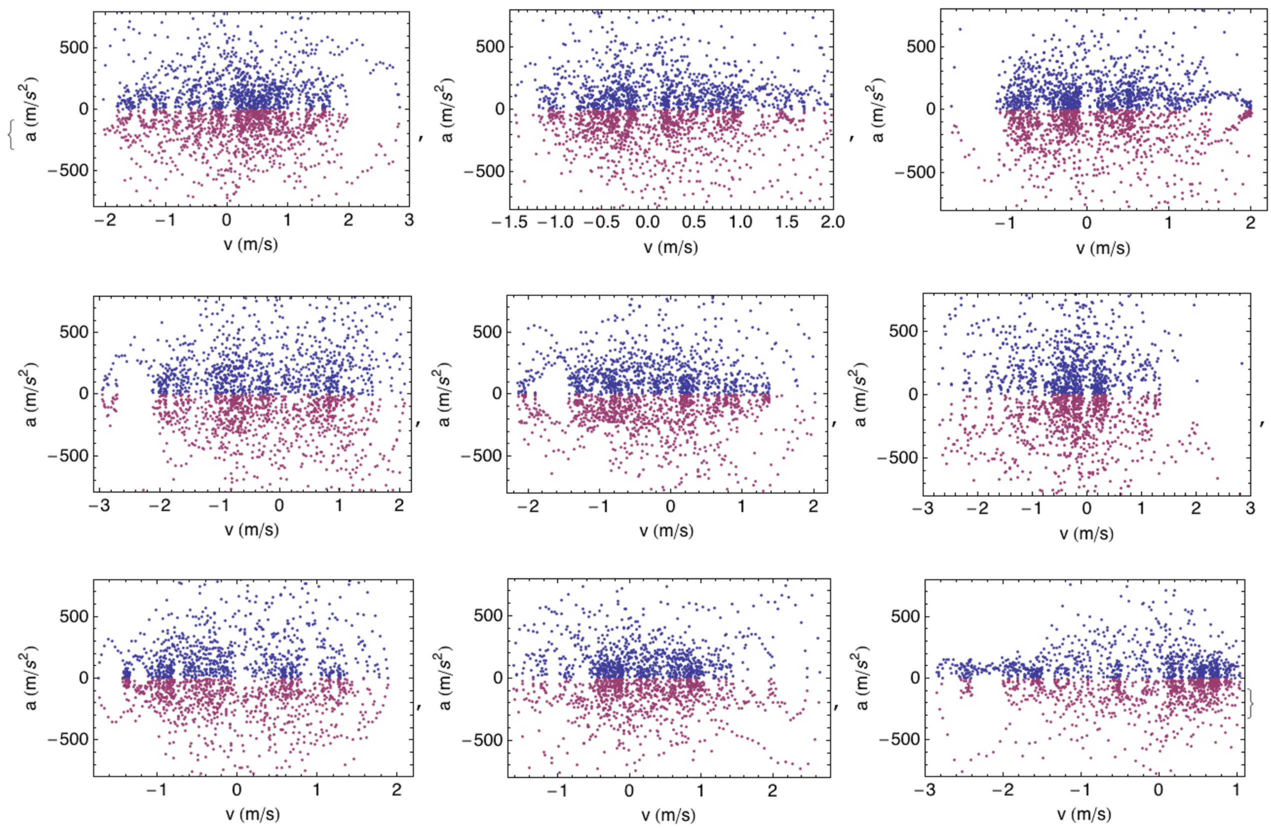

FIG. 10. Examples of "phase" diagram (v, a) for nine long segments of Mordant's experiment man290501 (respectively, segments 1135, 2578, 3030, 85, 3439, 8292, 9508, 6353, and 3500, whose length vary from 2218 to 1729 t_u, i.e., ≈1700 to 1300 τ_η and ≈15 to 12 T_l). One can easily check that the existence of almost empty minima in the velocity distribution for $|a| < \approx\sigma_a$ = 280 m/s^2 is a systematic property of these Lagrangian segments although the position of these minima varies, as expected, from one segment to the other. On the contrary, the velocity PDFs for $|a| > \approx \sigma_a$ remains smooth and close to Gaussian (see Fig. 13).

$P_v^q(v)$. Setting $\delta v = v - v_i$, one may write to lowest order approximation $P_v^q(\delta v) \sim \delta v^2$ so that $A_q = 2\mathcal{D}_v/\delta v$ (blue dashed curve in Fig. 11). The minimum is expected to be not strictly null in real data so that one may write $P_v^q(\delta v) = P_0[1 + (\delta v/w)^2]$ around the minimum. Therefore, one obtains an improved formula (red curve in Fig. 11)

$$A_q(\delta v) = \frac{2\mathcal{D}_v \delta v}{w^2 + \delta v^2}. \tag{41}$$

The effect of the small threshold w is to cut-off the divergence in $\delta v = 0$. In this model, we expect the value of A_q to go down to 0 in the center of the P_v minimum at $\delta v = 0$. A cutoff of the divergence can also be directly inserted in the acceleration by writing $A_q = 2\mathcal{D}_v/(\sqrt{w^2 + \delta v^2})$. In this expression, the acceleration no longer vanishes at $\delta v = 0$, while it shares the same behavior as the previous ones at large δv's (black curve in Fig. 11).

These expressions remain somewhat unrealistic since they do not take the local maxima of P_v into account. This can be locally modeled by writing

$$P_v = P_0\left[1 + \left(\frac{v_1}{w}\right)^2 \sin^2 \frac{\delta v}{v_1}\right], \tag{42}$$

leading to the expression (dashed brown curve in Fig. 11)

$$A_q(\delta v) = 2\mathcal{D}_v \frac{v_1 \cos(\delta v/v_1)\sin(\delta v/v_1)}{w^2 + v_1^2 \sin^2(\delta v/v_1)}. \tag{43}$$

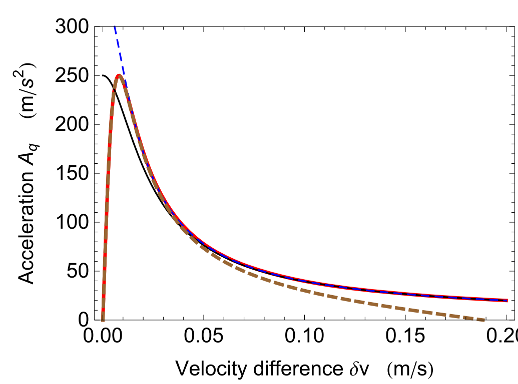

FIG. 11. Various models for the magnitude of the new acceleration component, $|A_q|(\delta v) = \mathcal{D}_v\, \partial \ln P_v(\delta v)/\partial(\delta v)$, in function of the distance δv to the nearest zero minimum of P_v. The dominant behavior is $|A_q| \propto \delta v^{-1}$, plus asymptotic possible corrections depending on the model (see text).

In this case, the new acceleration contribution vanishes at a distance $\pi v_1/2$ of the P_v minimum.

The existence of this new acceleration component can therefore be directly checked in Mordant's[37,44] experimental data. Actually, $A_q(v)$ is, by construction, defined at the smallest scale of the inertial zone, which is larger than the dissipative scale (due to the transition and, in Mordant's data, to the particle size). Therefore, its effect cannot be looked for directly on the individual data points (measured at time scale $\tau_u = 0.7\ \tau_\eta$), but instead on the whole arches themselves. For each segment, we identify the zero minima v_i in the velocity PDF. Then, we look for the maximal acceleration of the arches in function of the distance δv between the closest P_v minimum and the arch first points (we take the closest of its first three points).

The result is given in Fig. 12. Its successful comparison with the theoretically expected dependence of A_q in a function of δv strongly supports the $A_q = \pm \mathcal{D}_v\, \partial_v \ln P_v$ process. We define an amplification factor as the ratio between the maximal acceleration in the arch and the acceleration around the zero minima of P_v, given by A_q. The final effect depends on the amplitude of A_q given by the parameter $\mathcal{D}_v$ and on this amplification. The experimental result of Fig. 12 corresponds to an amplification $K = 2.4$ and to $\mathcal{D}_v \approx 2.5$.

The final variance balance shows that we have captured most of the acceleration (i.e., of the forces) contributions. For example, in Mordant's 2D data, the standard deviation of the residual accelerations in calm zones is $\sigma_{A\xi} \approx 110$–$130$ m s^{-2}, while $\sigma_{Aq} \approx 260$–290 m s^{-2} and $\sigma_a = 330$ m s^{-2}. Therefore, the basic Gaussian stochastic fluctuations contribute for 10%–15% of the variance and A_q for 65%–75%. Then, there is still probably a small missing component which contributes to 10%–25% of the variance. This is not unexpected since we have neglected the contribution to the acceleration that comes from the phase of the wave function. The approximation of a negligible phase contribution was supported by a description of the largest eddies in the cascade in terms of harmonic oscillator potentials, which leads to real solutions of the Schrödinger equation. It is clear that this cannot be strictly correct so that another small contribution is naturally expected, which is however difficult to estimate directly.

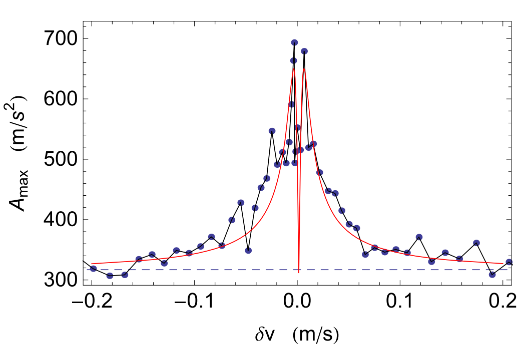

FIG. 12. Direct experimental proof of the new acceleration contribution $A_q(\delta v)$. The maximal acceleration in arches is plotted against the distance (in v-space) to the closest minimum of $P_v^q(v)$ [points, Mordant's 2D experimental data). It is compared to the theoretically expected relation $A_q(\delta v)$, which is ~$1/\delta v$ plus a cutoff toward the origin [Eq. (41), red curve, $w = 0.0055$ m/s].

C. Intermittency of acceleration

In a turbulent fluid, the accelerations show, in function of time, an alternance of calm periods followed by multiscale bursts of large accelerations (see Fig. 7). This behavior is a direct view of the intermittency of the turbulent flow (which is often characterized by non-K41 exponents of structure functions; see below).

The new acceleration contribution $A_q[v(t)] = \pm \mathcal{D}_v\, \partial_v \ln P_v[v](t)$ yields a detailed explanation and account of this behavior (see Figs. 13 and 14). We give in Fig. 13 an example of time evolution of velocity and acceleration for a segment of Mordant's data. This segment shows, as predicted, well defined peaks and almost zero minima of the velocity PDF for $a < \sigma_a$, while the PDF is close to Gaussian for $a > \sigma_a$ (left figure). This comes in support of a macroquantum to classical transition around σ_a.

Moreover, it is clearly seen in this figure that the calm periods correspond to the velocity oscillating into the main probability peaks, while the acceleration bursts result from jumps between these peaks (induced by the basic Gaussian underlying stochastic fluctuation), i.e., from the passage through the minima $P_v(v) \approx 0$ where the new acceleration component $A_q = \mathcal{D}_v\, \partial_v \ln P_v$ is expected to diverge.

In addition, we have performed a simulation which consists of (1) fitting an analytical velocity PDF $P_v(v)$ (given by an harmonic oscillator solution of the Schrödinger equation) on the observed PDF (for $|a| < \sigma_a$, left Fig. 13) in a long segment of Mordant's experiment; (2) computing an analytical expression $A_q(v) = \mathcal{D}_v\, \partial_v \ln P_v$ from this theoretical $P_v(v)$, assuming $\mathcal{D}_v$ =cst; (3) following the values $v(t)$ experimentally observed for this segment, and for each velocity at each time, computing $A_q[v(t)]$; (4) according to our model [Eq. (37)], we add a random Gaussian fluctuation $A_\xi(t)$ (of standard deviation only one third of that of A_q). We have neglected here the Langevin term, which contributes very weakly to the global variance. The result is given in Fig. 14 and compared to the observed time evolution of acceleration in this segment. The agreement between the two variations is striking (the intercorrelation between the observed and predicted accelerations is at the 10 σ level).

In the simulation whose result is shown in Fig. 14, the model PDF is that of a quantized harmonic oscillator with $n = 3$, $v_0 = 0.29$ m s^{-1} and mean velocity $v_m = -0.30$ m s^{-1}, which has been fitted to the "quantum" domain subsample $|a| < \sigma_a$ of a long segment (see Fig. 13). The added Gaussian fluctuation has a standard deviation $\sigma_{a_\xi} = 80$ m s^{-2} to be compared to the full standard deviation of the segment accelerations, $\sigma_a = 285$ m s^{-2}. Therefore, more than 90% of the variance comes from the Aq component itself. The value of the parameter $\mathcal{D}_v$ which defines the amplitude of $A_q[v(t)] = \mathcal{D}_v\, \partial_v \ln P_v[v](t)$ is $\mathcal{D}_v = 6$ in this simulation. This value actually includes an amplification factor by the arches (oscillators at the Kolmogorov viscous scale) and is in good agreement with the effective value obtained in Sec. VI B.

D. PDF of acceleration

The form of the new contribution A_q, which diverges in the minima of P_v, yields a natural explanation for the very large values observed for accelerations in turbulent fluids.[36] Moreover, one of the main consequences of the scale relativity model of turbulence is its ability to predict in a detailed way the shape of the acceleration PDF, including, in particular, its large tails.

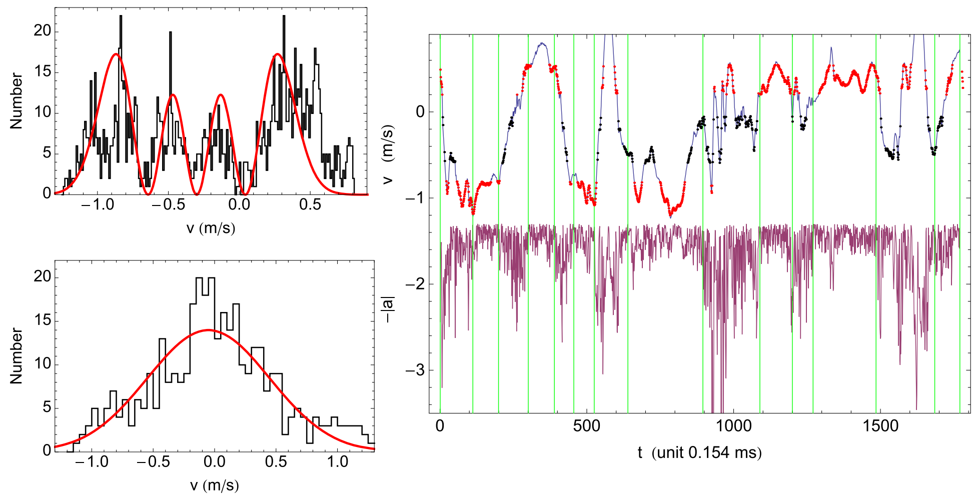

FIG. 13. Left figure: observed PDF of velocity for the subsample [1-1800] of Seg3398 of Mordant's experiment #3 (man290501). Top left figure: observed PDF of velocities for $|a| < \sigma_a$ (black histogram), compared with a solution of the macroscopic Schrödinger equation for a quantized harmonic oscillator with $n = 3$ (red curve). External peaks not accounted by this theoretical PDF just fit the corresponding classical oscillator. Down left figure: observed PDF of velocities for $|a| > \sigma_a$ (black histogram), compared with a Gaussian of standard deviation 0.7 m/s (red curve). Right figure: detailed analysis of the evolution of velocity and acceleration with time for the same subsegment. The top curve shows the time evolution of velocity $v(t)$. The bottom curve shows the time evolution of the acceleration magnitude ($|a(t)|$ (reversed, varying here from 0 to 1000 m/s^2). We have underlined in red the points lying in the main external peaks of the local PDF of velocity and in black those lying in the secondary internal peaks (top left figure). The vertical green lines mark the limit between the calm periods of acceleration ($\langle\sigma_a\rangle \approx 90$ m/s^2) and the intermittent bursts ($\langle\sigma_a\rangle \approx 330$ m/s^2).

The first step consists of deriving the PDF expected from the new acceleration $A_q = \pm\mathcal{D}_v\,\partial_v \ln P_v$, which is now the dominant contribution. The large tails of the PDF are simply explained by the fact that $P_v = |\psi_v|^2$ and that the modulus of the wave function ψ_v is expected to oscillate between positive and negative values. When it crosses $\psi_v = 0$ at some velocity v_i, one expects in most cases $\psi_v \propto \pm(v - v_i)$, and therefore $P_v \propto (v - v_i)^2$. Around these zeros, one gets $A_q = \pm 2\mathcal{D}_v/(v - v_i)$, which is divergent around $v = v_i$. This provides a simple explanation for the experimentally observed very large tails of the acceleration PDF. From this expression of A_q, it is easy to deduce the corresponding acceleration PDF in the tails,[29]

$$P_a(a) \propto \frac{1}{a^4}, \tag{44}$$

where a is the acceleration. One can easily improve this model by now describing both a local minimum in $\sim v^2$ and a nearby maximum of P_v in terms of a locally sinus function, $P_v(v) \propto \cos^2(v/v_0)$. Setting $\sigma_a = 2\mathcal{D}_v/v_0$, one obtains the acceleration PDF,

$$P_a(a) = \frac{2}{\pi\sigma_a}\,\frac{1}{[1 + (a/\sigma_a)^2]^2}. \tag{45}$$

Note that such a law has already been proposed by Beck[55,56] under the assumption of Tsallis statistics. (Recall that the Tsallis entropy

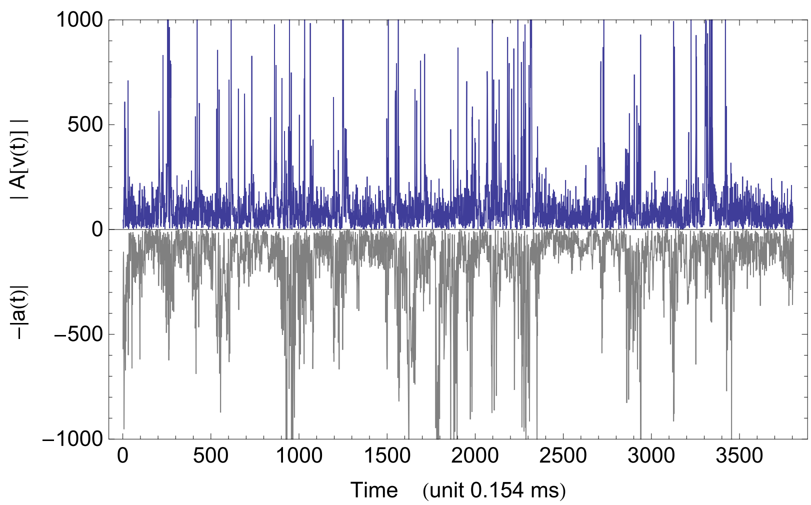

FIG. 14. Comparison between the values of $|A[v(t)]|$ predicted from the $A_q(v)$ acceleration component derived from a theoretical velocity PDF (blue curve, top figure, see text), with the experimentally observed evolution of the acceleration magnitude $|a(t)|$ for the whole segment Seg3398 of Mordant's experiment man290501 (gray curve, reversed, down figure). The velocity PDF used in the simulation is that of a quantized harmonic oscillator for $n = 3$ according to the fit of Fig. 13, the effective value of $\mathcal{D}_v$ is here $\mathcal{D}_v = 6$, and the added background Gaussian fluctuation has a standard deviation $\sigma_{a_\xi} = 80$ m s^{-2}. The main alternation of calm zones and acceleration bursts is clearly recovered in a very satisfactory way.

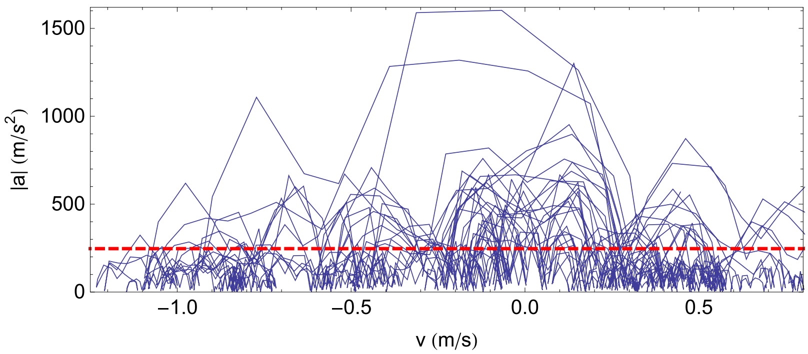

FIG. 15. The "phase" diagram $(v, |a|)$ in velocity space for the first part of seg3398 of Mordant experiment man290501 ($t = \tau_u$ to $1770\ \tau_u$). The straight lines connect the measurement points which are separated by $\tau_u = 1/6500$ s. The dashed line gives the local standard deviation of acceleration $\sigma_a = 245$ m/s^2 for this segment. The holes in the velocity PDF are clearly apparent for $a < \sigma_a$, while the large values of the acceleration ($a \gg \sigma_a$) evolve along "archs" which amplify the effect of the new acceleration component A_q.

is a nonadditive generalization of the standard Boltzmann-Gibbs entropy, while the associated statistics characterize complex, anomalous diffusion, and/or chaotic systems).

In our approach, it is directly predicted from the dynamics, but this is only a lowest order approximation, since this result is obtained from the mere behavior of the inertial range ($\delta v^2 \sim \delta t$). Despite this, it fits the experimental PDF very nicely up to about 15 sigmas (see Fig. 20).

Therefore, one should also account for the dissipative scales, which cut-off the acceleration divergence toward small time scales. For scales smaller than a few τ_η's, the scaling law $\delta v \sim \delta t^{1/2}$ is no longer valid and one comes back to a standard differential $\delta v \sim \delta t$. Therefore, toward small time scales ($\tau < \approx\tau_\eta$), the new acceleration contribution is no longer given by $A_q = \pm\mathcal{D}_v\, \partial_v \ln P_v$ with $\mathcal{D}_v$ constant. It tends to 0 when $\tau \to 0$ and becomes smaller than the stochastic fluctuation which is itself no longer scale-dependent. Therefore, at the limit $\tau \to 0$, one may write $\sigma_a^2 = 2\mathcal{D}_v/\tau$, where σ_a^2 is the asymptotic value of the acceleration variance, so that one obtains

$$A_q(\tau, v) = \frac{1}{2}\sigma_a^2\, \tau\, \partial_v \ln P_v(v). \tag{46}$$

One therefore expects the real acceleration PDF to be lower than the purely inertial a^{-4} law, as supported by the experimental data (see Fig. 16).

There are two consequences of this process. One direct consequence concerns the central part of the PDF ("small" accelerations, $|a| < 10\ \sigma_a$ in Bodenschatz *et al.* data,[7] $|a| < 4.5\ \sigma_a$ in Mordant's data due to the large particle size). By using the small scale expression of A_q [Eq. (46)], one finds a corrected law which can be integrated in terms of the special function MeijerG (given in Fig. 16),

$$P_a(A) = \int_0^\infty \exp\left(-2\,\frac{A}{t}\right)\frac{(1+t^2)^{-2}}{t}\,dt = \frac{1}{2\sqrt{\pi}}\, G_{1,3}^{3,1}\left(A^2 \middle| \begin{matrix} -1 \\ 0, 0, \frac{1}{2} \end{matrix}\right). \tag{47}$$

This function perfectly fits the experimental data in the central part of the PDF (see Figs. 16 and 20). Beyond a few σ_a's, it becomes identical to the a^{-4} law. Therefore, this effect does not impact the very large tails of the PDF.

There is a second indirect consequence of the existence of the dissipative transition which now applies to the large tails. The largest values of the acceleration are obtained at the smallest time scales, i.e., in the dissipative eddies at sub-Kolmogorov scales. These eddies can be described in terms of damped harmonic oscillators (DHO) (in v-space), which are solutions of the equation

$$\frac{da}{dt} = -\frac{a}{T_a} - \frac{(v - v_0)}{\tau_\omega^2}. \tag{48}$$

One can show (see the Appendix) that this simple model yields solutions that are very close to the anharmonic oscillators directly obtained from the Navier-Stokes equations at dissipative scales, $dv/dt = \nu\Delta v$. These damped solutions achieve "arches" (see Figs. 15 and 18) whose shapes are characterized by the parameter

$$\chi = \frac{\tau_a}{4T_a} = \frac{\tau_\omega}{2\sqrt{4T_a^2 - \tau_\omega^2}}. \tag{49}$$

One finds for the arches, the general relation

$$\frac{A_{\max} T}{\pi\,\Delta V} = K(\chi) = 1 + \chi^2 + \ldots, \tag{50}$$

where $A_{\max}$ is the maximal acceleration reached on half a period, T is the half-period duration, and ΔV is the half velocity extension of the arch. Then, at small time scales close to the dissipative scales, the maximal acceleration $A_{\max} \propto A_q \propto \tau$. One identifies the scale variable τ to τ_a and since the damping time T_a does not depend on

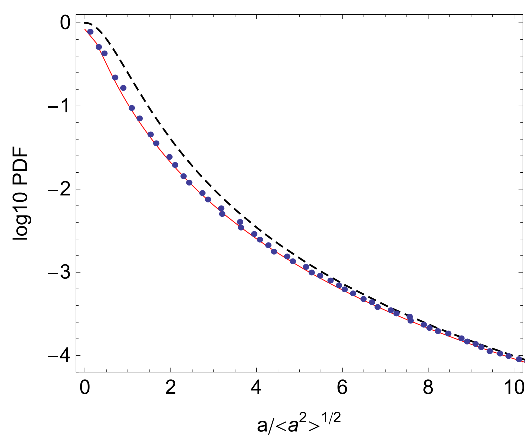

FIG. 16. Comparison between Mordant *et al.*[7] experimental data (blue points) in the "central zone" ($a < \approx 10\sigma_a$) of the acceleration PDF and the theoretical expectation accounting for the dissipative scales [Eq. (47), red continuous curve]. The dashed curve is the primary a^{-4} law predicted from the sole inertial (K41) range.

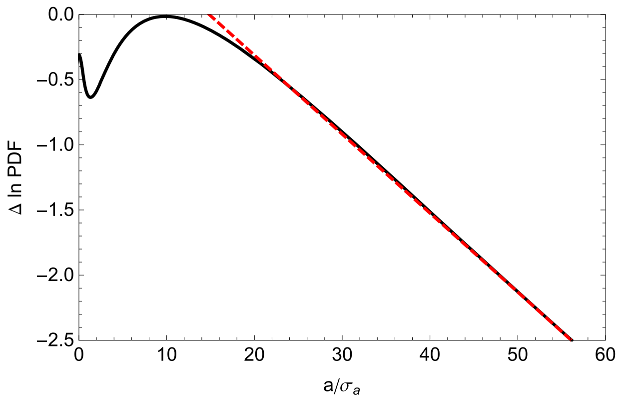

FIG. 17. Ratio between the Voth *et al.*[32] phenomenological formula (that fits the experimental acceleration PDF) and the a^{-4} law theoretically expected as a first order approximation (see text). The black curve is the difference between the logarithms of the two PDFs. It is compared to an exponential cutoff (red dashed line).

scale, one finds that $A_{\max} \propto \tau_a \propto \chi$. This means that the probability distribution of the arch shapes is not constant in function of their amplitude, but instead that their maximal acceleration is correlated with their shape. The larger the maximal acceleration, the larger the χ, i.e., the largest accelerations are obtained in arches (eddies) which are more damped. This expectation can be successfully checked in Mordant's data:[37] as can be seen in Fig. 19, there is a quadratic correlation for large accelerations $A_{\max} > 4\sigma_a$, between the parameter $K(\chi) \approx 1 + \chi^2$ and the maximal acceleration $A_{\max}$ at the 17σ level of significance, validating the theoretical expectation $A_{\max} \propto \chi$.

One naturally expects an exponential cutoff to the a^{-4} purely inertial law from such a relative damping mechanism. This is supported by the experimentally observed PDF (see Fig. 17).

Therefore, an acceleration which should have been A with an A^{-4} PDF without this effect is reduced to a smaller acceleration a by a damping factor $\rho(a) = a/A(a)$ (see Fig. 18). This damping factor can be established from the analytical expressions of the arches obtained from solving the viscous Navier-Stokes equation at dissipative scales, $dv/dt = \nu\Delta v$ (see the Appendix).

As expected, this process results in an exponential cutoff to the PDF tails, such that the corrected PDF is found to be given, for Bodenschatz *et al.* data,[7] by

$$P_a(a) \propto \frac{e^{-2\sqrt{1+(a/26.7\sigma_a)^2}}}{[1+(a/\sigma_a)^2]^2}, \tag{51}$$

where the numerical coefficient results from a fit of the experimental data.

The corresponding PDF for Mordant data[37] is obtained from a simple dilation of the acceleration values, $a_B \approx 2.3\ a_M$ which accounts for the particle size effect (amounting to an effective Kolmogorov scale $\tau_{\eta\text{eff}} \approx 5\ \tau_\eta \approx 2.3^2 \tau_\eta$). Note that, in the observed range ($|a| > \approx 15\ \sigma_a$ in Bodenschatz *et al.* data), this exponential cutoff is indistinguishable from the simple following law, depending on only one free parameter a_0,

$$P_a(a) \propto \left(\frac{1}{a} - \frac{1}{a_0}\right)^4, \tag{52}$$

where a is normalized to σ_a. The free parameter is fitted to $a_0 = 44$ for Mordant's data and $a_0 = 100$ for Bodenschatz *et al.* data (in agreement with the ratio ≈2.3 between the two sets of data).

It has been shown[32,7] that the experimental acceleration PDFs, once normalized, exhibit universal behavior for high Reynolds numbers ($R_\lambda > \approx 500$) and can be well fitted by a phenomenological stretch exponential formula. Our resulting predicted PDF shows an excellent agreement, with only one fitted parameter, with both this phenomenological fit and the experimental data (see Fig. 20).

E. Gaussianity of residual fluctuations in calm zones

One of the most radical new predictions of the scale relativity model of turbulence is that the residual fluctuations, beyond the effect of A_q, remains Gaussian. This is opposite to the standard description in which, except for the small Langevin term, the whole acceleration is stochastic and should therefore be characterized by the highly non-Gaussian PDF with large tails.

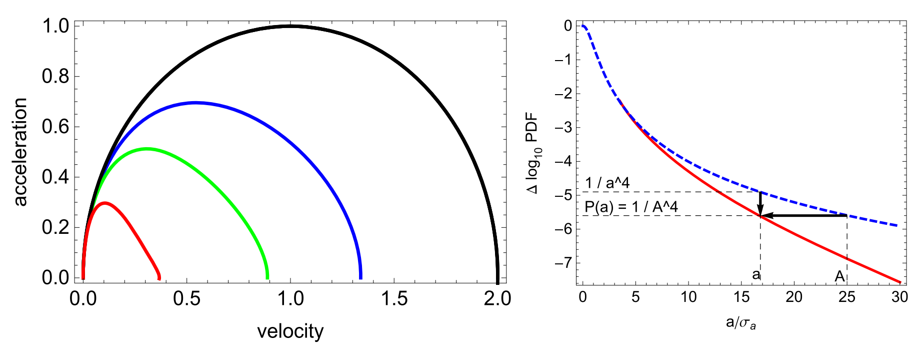

FIG. 18. Illustration of the mechanism of exponential cutoff to the a^{-4} law (first order approximation of the acceleration PDF). Left figure: a decrease in the maximal acceleration reached for similar initial conditions (the acceleration scale is here arbitrary), in function of the damping parameter χ: from top to down, $\chi = 0$ (harmonic oscillator, highest black curve), $\chi = 0.2$ (blue curve), $\chi = 0.4$ (green curve), and $\chi = 0.8$ (lowest red curve). Right figure: an acceleration which should have been A with an A^{-4} PDF according to the inertial regime is decreased to $a = \rho(A)\,A$ due to the damping mechanism of the left figure. Since χ is correlated with A (see text), the depletion is larger for higher accelerations.

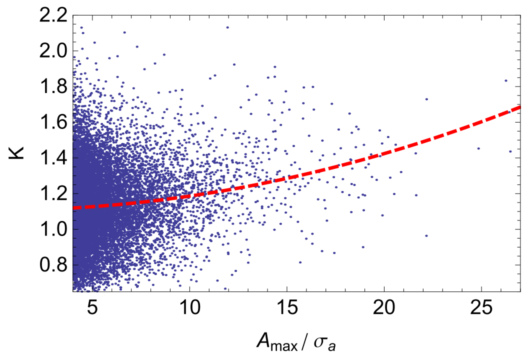

FIG. 19. Experimentally observed quadratic correlation between the parameter $K(\chi) = \pi^{-1}A_{max}T/\Delta V \approx 1 + \chi^2$, which characterizes the shape of the "arches" [anharmonic or damped oscillator solutions of the viscous Navier-Stokes (NS) equation, see (A7), with $K = 1$ for the harmonic oscillator] and their maximal acceleration A_{max} (Mordant experiment man290501). One finds a regression curve $K(x) = 1.107 + (x/35.46)^2$, where $x = A_{max}/\sigma_a$ (red dashed curve), significant at the 17 σ level, thus supporting the expectation that $A_{max} \propto \chi$.

In our model, the large tails are generated by A_q, while the stochastic residual fluctuation A_ξ is expected to be a standard Gaussian Brownian motion with variance $\sigma^2_{A_\xi} \ll \sigma^2_a$.

It is easy to check for this property in experimental data since we expect the acceleration to be reduced to the fluctuation A_ξ when A_q vanishes, and we know precisely when this occurs: just when the velocity v is far from the zero minima of P^q_v, namely, when the particle trajectory oscillates inside the probability peaks of the velocity PDF, without crossing the null minima (see Fig. 13). This corresponds to the "calm" zones of the intermittent acceleration (see, e.g., Fig. 6).

This expected correlation is supported by a statistical analysis of Mordant's experimental data: in the 2D data (which allows us to correct for the $v = 0$ bias present in the 1D data), we find that 85% of the calm zones are inside the probability peaks of $P^q_v(v)$ ($|a| < \sigma_a$).

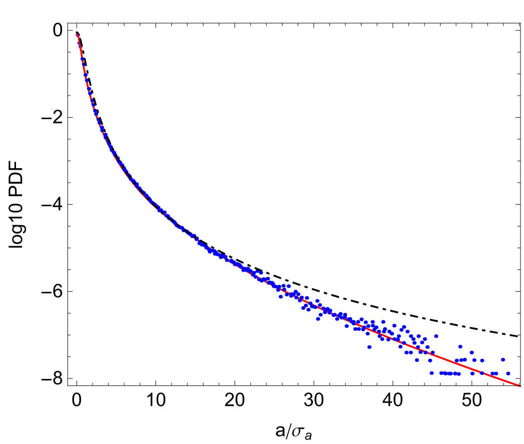

FIG. 20. Comparison between the observed acceleration PDF in Bodenschatz *et al.* data[7] (R_λ = 690, 10^8 values up to ~55 sigmas, blue points), the $(1 + (a/\sigma_a)^2)^{-2}$ law expected as a first approximation (dotted-dashed black curve), and the PDF corrected for both small and large accelerations (red continuous curve). The corrected curve perfectly fits the data within experimental uncertainties.

We give in Fig. 21 the PDF of acceleration in these calm zones in Mordant's experimental data. It is fully Gaussian with a high level of precision, showing absolutely no non-Gaussian large tail. Its standard deviation is $\sigma_{A\xi} = 115$ m s^{-2} which is 40% of the full $\sigma_a = 280$ m s^{-2}. In other words, the residual Gaussian fluctuation contributes to now only ≈16% of the variance and therefore A_q to ≈84% or less [since a small missing phase term may also contribute; see Eq. (32) and what follows].

F. Autocorrelation functions of acceleration modulus

One of the most interesting results of recent experimental turbulence studies is the discovery of a linear long-range behavior for the square root of the autocorrelation function $R^{1/2}_{|a|}$ of the acceleration modulus (see right Fig. 22). A similar result holds for the correlation function of its logarithm, $R_{\ln|a|}$ (right Fig. 23).[37,44] This result is used as empirical basis for multifractal random walk models[10,11,9,1] which have allowed to recover, e.g., the values of some of the exponents of structure functions.

These models are just built from the assumption of an autocorrelation of the acceleration magnitude given by[44]

$$\langle \ln|A(t)|\ \ln|A(t+\tau)|\rangle = -\lambda^2 \ln\frac{\tau}{T_L}, \tag{53}$$

where $\tau = \delta t < T_L$ and λ^2 is an adjustable parameter.

We have performed numerical simulations of the Schrödinger/A_q process [Eq. (37)] and then computed $R^{1/2}_{|a|}$ and $R_{\ln|a|}$ for the accelerations obtained in these simulations. Some typical examples of the results are given in the left parts of Fig. 22 and Fig. 23. We obtain the same results independently of the chosen value for the quantum number n characterizing the oscillator in the Schrödinger equation. This independence is expected since the dominant effect comes from the minima of $P^q_v(v)$ which have a universal parabolic shape. The simulations look very much like the experimentally observed autocorrelation functions (right figures), with values of the slope close to the observed one $-\lambda^2 \approx -0.12$. This suggests that a universal process may be at play and that it should be possible to get an analytical expression of these autocorrelation functions.

G. Exponents of structure functions

One traditional way of characterizing intermittency is by the difference of observed exponents of the structure functions with respect to their expected K41 values.

Up to now, there is no available theoretical prediction of the values of these exponents in the present approach based on the effect of the new A_q acceleration component. Thus, we have achieved numerical simulations of the A_q-Schrödinger process, which provides us with virtual Lagrangian trajectories (in terms of sequences of velocity values) that we can compare with the real trajectories obtained in Mordant's experiments.[37,44] In these simulations, the velocity increment simply contains three components [Eq. (34)]: a Langevin term $-v dt/T_L$ which ensures the velocity autocorrelation, the new component $A_q(v)dt$, and a Gaussian random fluctuation.

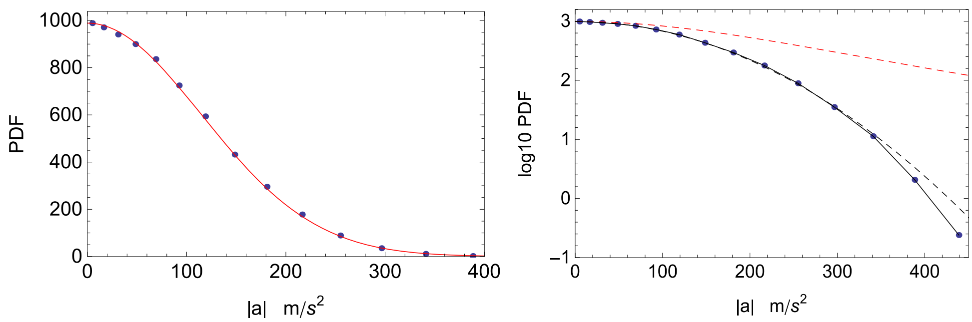

FIG. 21. Left figure: observed PDF of accelerations in the calm zones (points, from Mordant 2D experiment[37]), compared with a Gaussian (red curve). Right figure: logarithm of this PDF, confirming its Gaussian nature (black dashed curve) and the absence of large tails, compared to the a^{-4}-like global PDF (red dashed curve).

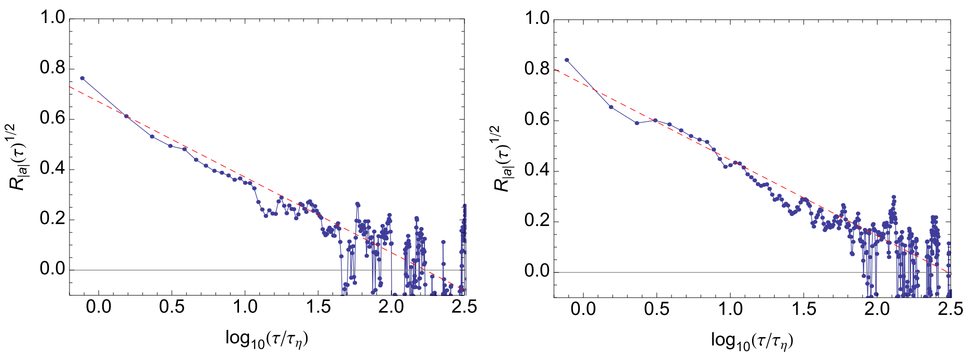

FIG. 22. Square-root of the autocorrelation function $R_{|a|}^{1/2}$ of the acceleration magnitude. The left figure is obtained from a numerical simulation of the acceleration values $A_q[v(t)]$ derived from a velocity PDF given by a $n = 3$ quantized harmonic oscillator. It compares very well with the right figure, which is obtained from the experimental values of acceleration for Seg3398. The dashed red lines are linear fits with yield similar slopes in the simulation and in the experimental data.

The function $A_q(v)$ is given by the solution of the Schrödinger equation [Eq. (37)] in harmonic oscillator potentials with various values of the quantum number n.

Our goal here is just to compare the structure functions and their scale exponents in the simulated data with those of the experimental data so that we have applied to the simulation the same method of data analysis as used by Mordant *et al.*[37,31,44]

Then, we have computed the structure functions in the simulations,

$$D_p(\tau) = \langle |\Delta_\tau v|^p \rangle. \tag{54}$$

Then, we have established their scale dependence (see Fig. 24) and measured the exponents p through Extended Scale Similarity (ESS),[57] in which one looks for the scale dependence of the structure functions relatively to the second order moment D_2, i.e., $D_p(\tau) = D_2(\tau)^{\xi_p}$.

The result is compared in Fig. 25 to the exponents measured by Mordant in his experimental data.[37,44] The experimentally measured exponents are closely reproduced (within uncertainties) by the simulation, even for large values of $p > 4$ for which the various existing models no longer account properly for them.[58]

Besides the simple (experimental vs simulated) data analysis given here above, one may briefly discuss the question of the validity of the exponents determination. It has been shown that the exponents actually depend on the Reynolds number so that finite Reynolds effects should be taken into account.[2] The second

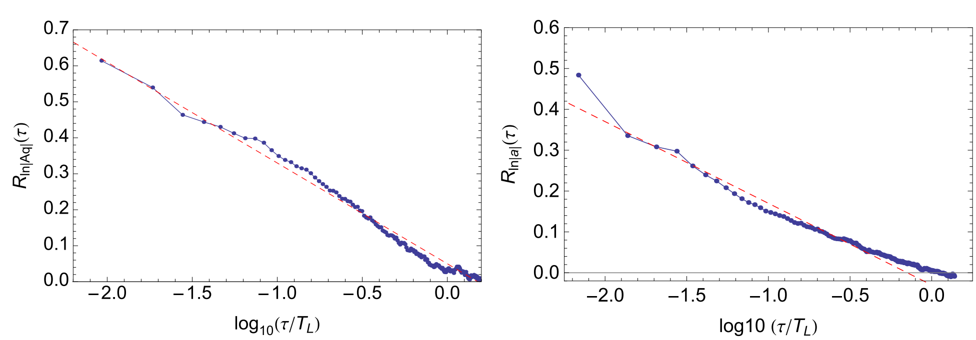

FIG. 23. Autocorrelation function $R_{\ln|a|}(\tau)$ of the logarithm of the acceleration magnitude. The left figure is obtained from a numerical simulation of the acceleration values $A_q[v(t)]$ derived from a velocity PDF given by a $n = 1$ quantized harmonic oscillator. The simulated trajectory has been smoothed to account for the particle size in Mordant's experiments. The resulting autocorrelation function compares well with the right figure, which is obtained from the experimental values of acceleration for Mordant's experiment man290501. The red dashed lines are linear fits which yields similar slopes in the simulation and in experimental data.

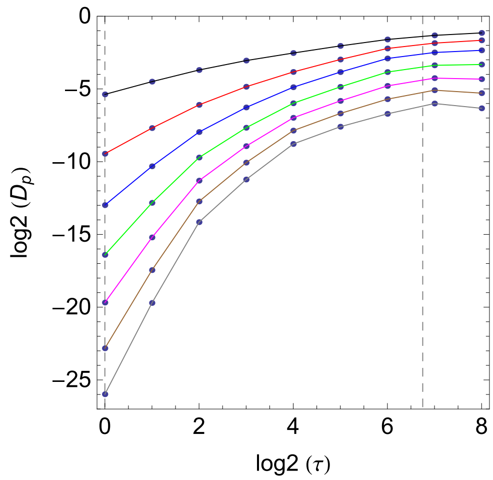

FIG. 24. Structure functions obtained in a numerical simulation of the A_q-Schrödinger process, D_1 to D_7, from top to down. The velocity PDF is solution of a Schrödinger equation for a harmonic oscillator potential with $n = 3$. The trajectory in the simulation contains $N = 80\,000$ points sampled with time intervals τ_η and then smoothed with a filter of width $5\tau_\eta$ to account for a particle size 250 μm, as in Mordant's experiment. The simulated structure functions are in close agreement with those obtained from the experimental data in this experiment.[37,44]

question is on the validity of the ESS method applied to the Lagrangian case. ESS has been discovered[57] to be an extension of the multifractal approach introduced by Frisch *et al.* (see, e.g., Ref. 1), and it has been applied to flows in the Euler formulation of the NS equation. It seems to be valid at any Reynolds number, and it relies on the 4/5 law involving the 3rd order correlation function in space. However, ESS has been also applied by Mordant *et al.* in the Lagrangian case, now starting from the second order structure function in time, under the Multifractal Random Walk hypothesis. This procedure was not justified at that epoch by these authors who used it as an ansatz, but it was found useful for comparing the predictions

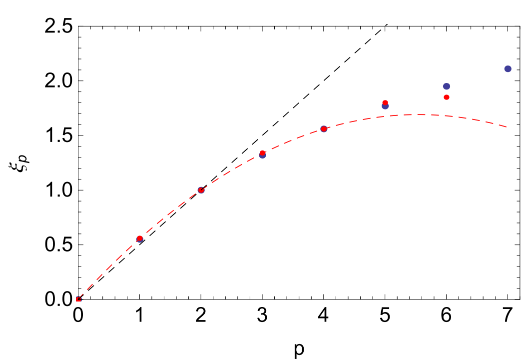

FIG. 25. The exponents of the structure functions measured in a numerical simulation of the Schrödinger-A_q process for a harmonic oscillator potential with $n = 3$ (blue points) are compared to those measured in experimental data ([37] smaller red points) to the K41 expectation (black dashed line) and to the exponents derived from a multifractal random walk model (Ref. 11, red dashed curve).

of this model on the exponents of the structure functions to the new Lagrangian experimental data.

The relation between the Eulerian and Lagrangian exponents in the multifractal model is now established.[58,59] Moreover, the application of the ESS to the Lagrangian case has been now substantiated.[60,61] More recently a mathematical study by Drivas[62] gave a rigorous equivalent of the 4/5 law in the Lagrangian case involving the second order structure function. From this relation, one can now reliably construct an ESS method valid in the Lagrangian case.

VII. DISCUSSION AND CONCLUSION

Let us explain in more detail the mechanism underlying the new process. The inertial range and its K41 scaling law $\delta v^2 \sim \delta t$ serves as microscopic structure and theory for the establishment of the Schrödinger equation. The oscillator potential in this equation therefore corresponds to the largest eddies of the cascade, at the large scale end of the inertial domain. These large eddies remain established during times that may be far larger than the integral time T_L (a full turn of the particle in the eddy lasts $\approx \pi t_L = \pi L/\sigma_v \approx 6$–$9\ T_L$ and several turns are possible). This explains why a macroquantum structure may exist on times $\gg T_L$.

Then, the new acceleration component A_q is generated from the solution $P_v^q = |\psi|^2$ of this Schrödinger equation. It is expected to describe the observed PDF only for $|a| < \approx\sigma_a$ since there is a macroquantum to classical transition around σ_a. The experimentally observed PDF is a mixing of macroquantum and classical contributions. We expect these solutions of a Schrödinger equation to be manifest only in Lagrangian data and only "locally" (i.e., on a given unique trajectory or segment of trajectory of a fluid element). Indeed, the combination of different Lagrangian trajectories smoothes out the Schrödinger structures due to shift of the minima and maxima of P_v for different oscillator potentials describing different eddies. In the same way, the Eulerian data correspond to different trajectories for each measurement, involved in different eddies, thus preventing from manifesting the expected structures.

The scale where A_q is established is the lowest end of the inertial range, just larger than the viscous Kolmogorov scale τ_η. At dissipative scales, below τ_η, one recovers a standard differential regime $\delta v \sim \delta t$, and the particle trajectories become again deterministic. They are involved in dissipative eddies well described by classical damped or anharmonic oscillators. Although these eddies have the smallest radii and velocities, their accelerations are the largest of the cascade. These "arches" achieve a kind of amplification to very large accelerations $a \gg \sigma_a$ of the A_q component generated in the macroquantum domain.

Let us finally recall the key-points of the new scale relativity approach to turbulence:

(1) Under fractal and nondifferentiable conditions, the derivative of the Navier-Stokes equations can be transformed, in the inertial domain, into a Schrödinger-type equation;
(2) The velocity PDF, $P_v = |\psi_v|^2$, is obtained from a "local" solution ψ_v (i.e., concerning one segment of trajectory of a fluid particle) of this macroscopic Schrödinger equation (in the sense that the constant which replaces $\hbar$ is a macroscopic diffusion coefficient). This Schrödinger regime is valid for $|a|$

$< \approx\sigma_a$, beyond which there is a transition to classical behavior (which is a manifestation of the de Broglie transition in v-space).

(3) The fact that P_v is the square of the modulus of the "wave function" ψ_v implies that null minima $P(v_i) = 0$ must exist for some values of the velocity. An analysis of Mordant's experimental data has allowed us to show that the velocity PDFs of individual Lagrangian segments are indeed highly non-Gaussian and present in a systematic way empty zones in the "macroquantum" domain $|a| < \approx\sigma_a$. This quasitotal exclusion of some particular values of the velocity appears as a highly nonclassical feature. This nonstandard behavior is re-enforced by the fact that the velocity PDF remains near to Gaussian when $|a| > \approx\sigma_a$, i.e., beyond the expected macroquantum to classical transition.

(4) The existence of a new acceleration component $A_q = \pm\mathcal{D}_v\,(\partial_v P_v)/P_v$ is deduced from this model. Due to its $1/P_v$ dependence, this new component is divergent at the quasinull minima $P_v(v_i) \approx 0$. This explains the very large values observed for accelerations in turbulent fluids. This new component has been directly seen and validated in the experimental data.

(5) Moreover, the general behavior of the velocity PDF around its minima, $P_v \sim \delta v^2$, allows one to derive a universal shape for the acceleration PDF under a pure inertial regime, $P_a(a) \sim 1/a^4$. The account for the Kolmogorov dissipative range leads to correct this law in terms of an exponential cutoff at large accelerations. The finally obtained PDF perfectly fits the experimentally observed one with only one free parameter, including its very large tails (which have been measured up to $\approx 55\,\sigma_a$).

(6) The predicted existence of an alternance of probability peaks and of almost empty minima in the velocity PDF of individual segments also accounts for the intermittency of acceleration in great detail. When the particle velocity oscillates inside one of the probability peaks without crossing a minimum, the A_q contribution remains small and only the stochastic fluctuation remains. This leads to the calm zones of the intermittent acceleration. Since the highly non-Gaussian statistics of acceleration is fully accounted for by A_q, the residual fluctuation is expected to be strictly Gaussian. This expectation is fully supported by experimental data. As concerns the intermittent bursts, they are predicted to result from "quantum jumps" between the probability peaks, when the particle velocity crosses the zero minima, involving a divergence of the acceleration component A_q. There too, this process can be followed in detail in the experimental data.

(7) Finally, this analytical approach has been completed by numerical simulations of the Schrödinger/A_q process. They have allowed us to recover the experimentally observed autocorrelation functions of acceleration magnitude and the observed exponents of the structure functions.

We conclude by emphasizing that the new approach based on scale relativity methods that we have developed here is not statistical in its essence, but partly deterministic (although based on an underlying stochastic fluctuation). When a given large scale eddy is established for some time, its corresponding potential is determined and so is the solution of the Schrödinger equation including this potential. Then, P_v is known and finally the derived acceleration component $A_q(v)$. In practice, the complexity of the evolution of the velocity $v(t)$ leads to a pseudorandom nature of $A_q[v(t)]$: this explains why the intermittent acceleration in turbulent fluids has been considered up to now to be fully stochastic in nature. Another aspect of the present work is that, besides the new insights it brings on the nature of turbulence, it provides, if confirmed, a laboratory experimental validation of the theory of scale relativity (in its "macroquantum" aspects).

ACKNOWLEDGMENTS

We are extremely grateful to Dr. Nicolas Mordant for kind communication of his experimental data on Lagrangian measurements in turbulent flows. We also acknowledge useful remarks by two referees having allowed us to improve the paper.

APPENDIX: EXACT OSCILLATOR SOLUTIONS OF VISCOUS NS EQUATION AT KOLMOGOROV DISSIPATIVE SCALES

At Kolmogorov dissipative scales $\tau < \approx\tau_\eta$, where viscous effects become dominant, the Navier-Stokes equations take a simplified form

$$\partial_t u = \nu\,\Delta u, \tag{A1}$$

under the approximations $\nabla p \ll \nu\,\Delta u$ and $u\,\nabla u \ll \nu\,\Delta u$. These approximations both amount to neglecting second order contributions to the velocity, $u^2 \ll u$, where $u = u(x, y, z, t)$ is the Eulerian velocity field.

The Eulerian velocity $u[x, t]$ is by definition the velocity of the Lagrangian fluid particle which goes through position x at time t. Let us describe by $x_L(t)$ the trajectory of a fluid particle. The differential equation of the Lagrangian trajectory is given from the Eulerian velocity field by the equation

$$\frac{dx_L}{dt} = u[x_L, t]. \tag{A2}$$

We shall obtain one-dimensional solutions of this equation that are expected to be applicable to a fully developed turbulent fluid at scales around and lower than the Kolmogorov scale. Our results are easily generalizable to the 2D and 3D cases.

Oscillating solutions of Eq. (A1) have been obtained by Landau[5] although in a different context. They read, in terms of the Eulerian velocity field,

$$u[x, t] = \exp\left(-\frac{x}{\delta}\right)\exp\left\{i\left(\frac{x}{\delta} - \frac{t}{\tau_\delta}\right)\right\}, \tag{A3}$$

where the length-scale δ is linked to the time scale τ_δ by the relation

$$\delta = \sqrt{2\,\nu\,\tau_\delta}, \tag{A4}$$

where ν is the viscosity coefficient. These well-known solutions are characterized, as expected, by a (here spatial) damping Langevin-type term $-x/\delta$, typical of the dissipative process, and by a harmonic oscillator term.

The new result obtained here is that Lagrangian trajectories $x_L(t)$ can be derived from the Eulerian velocity field using Eq. (A2). We get a differential equation which we write in terms of reduced variables $X = x_L/\delta$ and $T = t/\tau_\delta$,

$$\dot{X} = e^{-X+i(X-T)}. \tag{A5}$$

Since we are interested here in the velocity aspect of the solutions, let us transform Landau's expression into a differential equation for $V = V/v_\delta$, where $v_\delta = \delta/\tau_\delta$. It reads (in terms of the acceleration $A = \dot{V} = dV/dt$)

$$A = -i\,V + (-1+i)\,V^2. \tag{A6}$$

This equation is easily solved under the form of an inverse harmonic oscillator, i.e., re-inserting the reference scales,

$$v(t) = \frac{u_0}{(1+i) + k\,\exp(i\,t/\tau_\delta)}, \tag{A7}$$

where k is a numerical integration constant.

There are many ways to express real solutions of the viscous NS equation deduced from the above general complex solution. An example is the following expression, from which the other solutions can be derived using the symmetries of the problem:

$$v(t) = \Delta v\left(h - (1-h^2)\frac{\cos(t/\tau_\delta) + h}{1 + h^2 + 2h\cos(t/\tau_\delta)}\right), \tag{A8}$$

where h is another integration constant. The acceleration reads

$$a(t) = \frac{\Delta v}{\tau_\delta}\,\frac{(1-h^2)^2\sin(t/\tau_\delta)}{[1 + h^2 + 2h\cos(t/\tau_\delta)]^2}. \tag{A9}$$

A power series expansion of $v(t)$,

$$v(t) = \cos\left(\frac{t}{\tau_\delta}\right) + h\left[1 - 2\cos^2\left(\frac{t}{\tau_\delta}\right)\right] + h^2\left[4\cos^3\left(\frac{t}{\tau_\delta}\right) - 4\cos\left(\frac{t}{\tau_\delta}\right)\right] + \ldots \tag{A10}$$

allows us to manifest the nature of these solutions as being actually anharmonic oscillators.

This exact oscillator solution of the viscous NS equation (NSO) can finally be compared with a damped harmonic oscillator (DHO) characterized by $\kappa = 2\chi = \tau_a/(2T_a)$ [Eq. (48)]. To this purpose, we identify the expressions of $A_{\max}/\Delta v$ obtained, respectively, in these two cases,

$$A_{\max-\mathrm{NSO}} \approx \frac{\Delta v}{\tau_\delta}\,(1 + 4\,h^2), \quad A_{\max-\mathrm{DHO}} \approx \frac{\Delta v}{\tau_\delta}\left(1 + \frac{1}{4}\kappa^2\right), \tag{A11}$$

and we identify the two half-periods so that $\tau_\delta = \tau_a$.

To the lowest order, one can therefore make the identification $\kappa \approx 4h$, which becomes to a better approximation $\kappa = 4h(1 + h^2/2)$. For small values of the parameters, the NSO and the DHO are undistinguishable. Even for large values, such as shown in Fig. (26), the solutions of the damped oscillator equation and of the viscous Navier-Stokes equation remain similar. They provide good representations of the shape of arches observed in actual experiments, such as seen, e.g., in Fig. 16.

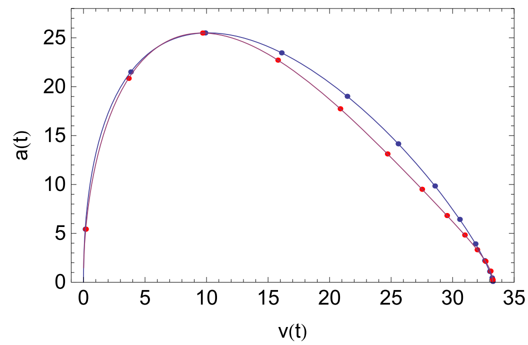

FIG. 26. Comparison in the (v, a) space on half a period ("arch") between the solution of the viscous NS equation (red lower curve) and a damped harmonic oscillator (blue upper curve) with same Δv and $A_{\max}$ and with $\tau_a = \tau_\delta$. The value of $\kappa = \tau_a/(2T_a) = 2\chi$ is $\kappa = 1.6$, and the corresponding value of h in Eqs. (A8) and (A9) is $h = 0.373$.

REFERENCES

[1] U. Frisch, *Turbulence: The Legacy of A.N. Kolmogorov* (Cambridge University Press, 1995).
[2] P. Sagaut and C. Cambon, *Homogeneous Turbulence Dynamics* (Springer, 2018).
[3] L. F. Richardson, "Atmospheric diffusion shown on a distance-neighbour graph," Proc. R. Soc. London A **110**, 709 (1926).
[4] A. N. Kolmogorov, "The local structure of turbulence in incompressible viscous fluid for very large Reynolds numbers," C. R. Acad. Sci. URSS **30**, 301 (1941).
[5] L. Landau and E. Lifchitz, *Fluid Mechanics* (Pergamon Press, Oxford, 1980).
[6] L. de Montera, "A theory of turbulence based on scale relativity," e-print arXiv:1303.3266 (2013).
[7] N. Mordant, A. M. Crawford, and E. Bodenschatz, "Experimental Lagrangian acceleration probability density function measurement," Physica D **193**, 245 (2004).
[8] A. N. Kolmogorov, "A refinement of previous hypotheses concerning the local structure of turbulence in a viscous incompressible fluid at high Reynolds number," J. Fluid Mech. **13**, 82 (1962).
[9] B. Castaing, Y. Gagne, and E. Hopfinger, "Velocity probability density functions of high Reynolds number turbulence," Physica D **46**, 177 (1990).
[10] A. Arneodo, S. G. Roux, and J. F. Muzy, "Experimental analysis of self-similarity and random cascade processes: Application to fully developed turbulence data," J. Phys. II **7**, 363 (1997).
[11] E. Bacry, J. Delour, and J. F. Muzy, "Multifractal random walk," Phys. Rev. E **64**, 026103 (2001).
[12] L. Biferale, G. Boffetta, A. Celani, B. J. Devenish, A. Lanotte, and F. Toschi, "Multifractal statistics of Lagrangian velocity and acceleration in turbulence," Phys. Rev. Lett. **93**, 064502 (2004).
[13] F. G. Schmitt and Y. Huang, "Analysis and simulations of multifractal random walks," in *Proceedings of 23rd European Signal Processing Conference (EUSIPCO)* (Nice, France, 2015), p. 1018.
[14] J. Friedrich, G. Margazoglou, L. Biferale, and R. Grauer, "Multiscale velocity correlations in turbulence and Burgers turbulence: Fusion rules, Markov processes in scale, and multifractal predictions," Phys. Rev. E **98**, 023104 (2018).
[15] M. Wilczek, H. Xu, N. T. Ouellette, R. Friedrich, and E. Bodenschatz, "Generation of Lagrangian intermittency in turbulence by a self-similar mechanism," New J. Phys. **15**, 055015 (2013).
[16] J. Friedrich and R. Grauer, "Generalized description of intermittency in turbulence via stochastic methods," e-print arXiv:1610.04432 (2016).
[17] D. Buaria, A. Pumir, E. Bodenschatz, and P. K. Yeung, "Extreme velocity gradients in turbulent flows," e-print arXiv:1901.09989 (2019).
[18] L. Nottale, *Fractal Space-Time and Microphysics: Towards a Theory of Scale Relativity* (World Scientific, Singapore, 1993).

[19] L. Nottale, *Scale Relativity and Fractal Space-Time: A New Approach to Unifying Relativity and Quantum Mechanics* (Imperial College Press, London, 2011).
[20] L. Nottale, *The Relativity of All Things* (Persistent Press, Nashville, 2019), updated English translation of *La relativité dans tous ses états* Hachette, Paris, 1998.
[21] B. Mandelbrot, *The Fractal Geometry of Nature* (Freeman, San Francisco, 1982).
[22] L. Nottale and M.-N. Célérier, "Derivation of the postulates of quantum mechanics from the first principles of scale relativity," J. Phys. A: Math. Theor. **40**, 14471 (2007).
[23] L. Nottale, "Scale-relativity and quantization of the universe. I. Theoretical framework," Astron. Astrophys. **327**, 867 (1997).
[24] L. Nottale, "Scale-relativity and quantization of extra-solar planetary systems," Astron. Astrophys. Lett. **315**, L9 (1996).
[25] L. Nottale, G. Schumacher, and E. T. Lefèvre, "Scale-relativity and quantization of exoplanet orbital semi-major axes," Astron. Astrophys. **361**, 379 (2000).
[26] C. Auffray and L. Nottale, "Scale relativity theory and integrative systems biology: 1 founding principles and scale laws," Prog. Biophys. Mol. Biol. **97**, 79 (2008).
[27] L. Nottale and C. Auffray, "Scale relativity theory and integrative systems biology: 2 Macroscopic quantum-type mechanics," Prog. Biophys. Mol. Biol. **97**, 115 (2008).
[28] P. Turner and L. Nottale, "The physical principles underpinning self-organization in plants," Prog. Biophys. Mol. Biol. **123**, 48 (2017).
[29] L. Nottale, "Relativity of scales, fractal space-time and quantum potentials," in *Space-Time Geometry and Quantum Events*, edited by I. Licata (Nova Science, 2014), Chap. 5.
[30] P. Turner and L. Nottale, "The origins of macroscopic quantum coherence in high temperature superconductivity," Physica C **515**, 15 (2015).
[31] N. Mordant, P. Metz, O. Michel, and J. F. Pinton, "Measurement of Lagrangian velocity in fully developed turbulence," Phys. Rev. Lett. **87**, 214501 (2001).
[32] G. A. Voth, A. La Porta, A. M. Crawford, J. Alexander, and E. Bodenschatz, "Measurement of particle accelerations in fully developed turbulence," J. Fluid Mech. **469**, 121 (2002); e-print arXiv: physics/0110027.
[33] R. Hermann, "Numerical simulation of a quantum particle in a box," J. Phys. A: Math. Gen. **30**, 3967 (1997).
[34] N. M. Qureshi, M. Bourgoin, C. Baudet, A. Cartellier, and Y. Gagne, "Turbulent transport of material particles: An experimental study of finite size effects," Phys. Rev. Lett. **99**, 184502 (2007).
[35] L. Nottale, "Macroscopic quantum-type potentials in theoretical systems biology," Cells **3**, 1 (2014); e-print arXiv:1306.4311.
[36] A. La Porta, G. A. Voth, A. M. Crawford, J. Alexander, and E. Bodenschatz, "Fluid particle accelerations in fully developed turbulence," Nature **409**, 1017 (2001).
[37] N. Mordant, "Lagrangian measurements in turbulence," Ph.D. thesis, Ecole Normale Supérieure de Lyon, 2001.
[38] G. Falkovich, H. Xu, A. Pumir, E. Bodenschatz, L. Biferale, G. Boffetta, A. S. Lanotte, and F. Toschi, "On Lagrangian single-particle statistics," Phys. Fluids **24**, 055102 (2012).
[39] R. C. Lien and E. A. D'Araso, "The Kolmogorov constant for the Lagrangian velocity spectrum and structure function," Phys. Fluids **14**, 4456 (2002).
[40] N. Mordant, E. Lévêque, and J.-F. Pinton, "Experimental and numerical study of the Lagrangian dynamics of high Reynolds turbulence," New J. Phys. **6**, 116 (2004).
[41] B. L. Sawford and P. K. Yeung, "Lagrangian statistics in uniform shear flow: Direct numerical simulation and Lagrangian stochastic models," Phys. Fluids **13**, 2627 (2001).
[42] N. T. Ouellette, H. Xu, M. Bourgoin, and E. Bodenschatz, "Small-scale anisotropy in Lagrangian turbulence," New J. Phys. **8**, 102 (2006).
[43] B. L. Sawford and P. K. Yeung, "Kolmogorov similarity scaling for one-particle Lagrangian statistics," Phys. Fluids **23**, 091704 (2011).
[44] N. Mordant, J. Delour, E. Lévèque, O. Michel, A. Arnéodo, and J.-F. Pinton, "Lagrangian velocity fluctuations in fully developed turbulence: Scaling, intermittency, and dynamics," J. Stat. Phys. **113**, 701 (2003).
[45] B. L. Sawford, "Reynolds number effects in Lagrangian stochastic models of turbulent dispersion," Phys. Fluids A **3**, 1577 (1991).
[46] M. S. Borgas and B. L. Sawford, "Stochastic equations with multifractal random increments for modeling turbulent dispersion," Phys. Fluids **6**, 618 (1994).
[47] S. B. Pope, "A stochastic Lagrangian model for acceleration in turbulent flows," Phys. Fluids **14**, 2360 (2002).
[48] L. Nottale, "Generalized quantum potentials," J. Phys. A: Math. Theor. **42**, 275306 (2009).
[49] L. Nottale and T. Lehner, "Numerical simulation of a macro-quantum experiment: Oscillating wave packet," Int. J. Mod. Phys. C **23**(5), 1250035 (2012).
[50] L. Landau and E. Lifchitz, *Quantum Mechanics* (Editions Mir, Moscow, 1965).
[51] C. Beck, "Superstatistical turbulence models," in Proceedings of MPA-Garching workshop 'Interdisciplinary aspects of turbulence', Tegernsee, 18–22 April 2005; e-print arXiv:physics/0506123.
[52] E. Krasnoff and R. L. Peskin, "The Langevin model for turbulent diffusion," Geophys. Fluid Dyn. **2**, 123 (1971).
[53] W. Heisenberg, "Zur statistischen theorie der turbulenz," Z. Phys. **124**, 628 (1948).
[54] A. M. Yaglom, "On the acceleration field in a turbulent flow," C. R. Akad. URSS **67**, 795 (1949).
[55] C. Beck, "Dynamical foundations of nonextensive statistical mechanics," Phys. Rev. Lett. **87**, 180601 (2001).
[56] C. Beck, "On the small-scale statistics of Lagrangian turbulence," Phys. Lett. A **287**, 240 (2001); e-print arXiv:physics/0105058.
[57] R. Benzi, S. Ciliberto, R. Tripiccione, C. Baudet, F. Massaioli, and S. Succi, "Extended self-similarity in turbulent flows," Phys. Rev. E **48**, R29 (1993).
[58] F. G. Schmitt, "Comment relier les exposants multifractals de la turbulence Eulérienne et Lagrangienne?," in Actes du 17ème Congrès Francais de Mécanique, Troyes, France, 2005.
[59] L. Chevillard, B. Castaing, A. Arneodo, E. Lévèque, J.-F. Pinton, and S. Roux, "A phenomenological theory of Eulerian and Lagrangian velocity fluctuations in turbulent flows," C. R. Phys. **13**, 899 (2012).
[60] A. Arneodo *et al.*, "Universal intermittent properties of particle trajectories in highly turbulent flows," Phys. Rev. Lett. **100**, 254504 (2008).
[61] K. P. Zybin, V. A. Sirota, A. S. Ilyin, and A. V. Gurevic, "Lagrangian statistical theory of fully developed hydrodynamical turbulence," Phys. Rev. Lett. **100**, 174504 (2008).
[62] T. D. Drivas, "Turbulent cascade direction and Lagrangian time-asymmetry," J. Nonlinear Sci. **29**, 65 (2019).